CATÓLICA
ESCOLA SUPERIOR DE BIOTECNOLOGIA
PORTO

PREPARATION, CHARACTERIZATION AND BIOLOGICAL EVALUATION OF HYBRID NANOSYSTEMS AS WOUND HEALING POTENTIATORS

by

Clara Tavares Miranda

November 2023

CATÓLICA
ESCOLA SUPERIOR DE BIOTECNOLOGIA
PORTO

PREPARATION, CHARACTERIZATION AND BIOLOGICAL EVALUATION OF HYBRID NANOSYSTEMS AS WOUND HEALING POTENTIATORS

Thesis presented to *Escola Superior de Biotecnologia of the Universidade Católica Portuguesa* to fulfill the requirements of Master of Science degree in Biomedical Engineering

by

Clara Tavares Miranda

Supervisor: Carla F. Pereira

Co-Supervisors: Óscar Leandro Ramos, João Azevedo Silva

November 2023

Resumo

Materiais híbridos constituídos por óxido de zinco e nanocelulose têm sido amplamente explorados para um número de aplicações considerável, incluindo propósitos relacionados a cicatrização de feridas ou como curativos. No entanto, as investigações desse potencial têm sido particularmente direcionadas a compostos híbridos constituídos por óxido de zinco e nanocelulose bacteriana, que é significativamente mais cara de obter devido à sua natureza.

Este trabalho visa a obtenção de compostos híbridos nanocelulose/ZnO que sejam seguros e sustentáveis para uso como materiais cicatrizantes. Para tal, foram exploradas condições de síntese *in-situ*, tendo-se usado os métodos hidrotérmico e sol-gel, onde se explorou o impato de diferentes parâmetros reacionais (rácio de reagentes; temperatura; tempo; métodos de lavagem e secagem) nas proprieadades estruturais dos materiais obtidos. A obtenção bem sucedida dos diferentes materiais foi atestada por espectroscopia de Ultravioleta-Visível (UV-Vis), os quais foram caraterizados a nível estrutural por: escpectroscopia de FT-IR (do inglês, Fourier Transform Infrared Spectroscopy) para estudo das vibrações caraterísticas da nanocelulose); por Raio-X de Pós (avaliação dos padrões de difração e cristalinidade) e por microscopia eletrónica, mediante utilização de SEM (do inglês, *Scanning Electron Microsccopy*) e TEM (do inglês, *Transmission Electron Microscopy*).

Os materiais híbridos de nanocelulose/ZnO obtidos que demonstraram robustez e caraterísticas estruturais diferenciadores foram estudados *in vitro* para determinação da concentração segura a partir de testes citotóxicos efetuados em células HaCaT, e o seu potencial de cicatrização de feridas foi também avaliado a partir de ensaio *in vitro*.

Palavras-chave: material híbrido; nanocelulose; óxido de zinco; síntese *in-situ*, cicatrização de feridas

Abstract

Hybrid materials comprising zinc oxide and nanocellulose have been widely explored for a good number of applications, including wound healing/dressing related purposes. However, investigation of wound healing materials has been more focused on bacterial nanocellulose-based zinc oxide hybrid composites, which utilize a form of nanocellulose that is significantly more expensive to obtain due to its nature.

This work aims the obtention of sustainable and safe nanocellulose-based zinc oxide hybrid composites as wound healing materials. For this purpose, *in-situ* synthesis' conditions were explored, employing *in-situ* hydrothermal and sol-gel synthetic approaches, where the impact of various reactional parameters (reagents ratio; temperature; time; washing and drying methods) on the structural properties of obtained materials was explored. Successful obtention of all different materials was attested via Ultraviolet-Visible (UV-Vis) spectroscopy, which were characterized on a structural level by: FT-IR (Fourier Transform Infrared) spectroscopy (for study of nanocellulose characteristic vibrations); by Powder X-ray analysis (evaluation of diffraction patterns and crystallinity) and by electronic microscopy, through SEM (*Scanning Electron Microsccopy)* and TEM (*Transmission Electron Microscopy*).

Obtained hybrid materials of nanocellulose/ZnO, that showed robustness and differentiating structural characteristics, were studied *in vitro* for determination of safe concentration through cytotoxicity tests performed on HaCaT cells, and their wound healing potential was also evaluated through *in vitro* assay.

Keywords: hybrid material; nanocellulose; zinc oxide; *in-situ* synthesis; wound healing potential

Aknowledgments

Primarily, I would like to express my sincere gratitude to my supervisor Carla Pereira who has given me great support in the writing process of this dissertation and with the experimental work. I would also like to thank you for the friendship and motivation given throughout the whole process.

To my supervisor João Azevedo Silva, I would like to thank you for your guidance, generosity and help in the laboratory.

For my supervisor Óscar Leandro Ramos, I would like to thank you for the advice and guidance provided in the past months.

To the PhD students Francisca Casanova and Nelson Mota de Carvalho, I would like to express my gratitude for the assistance with the experimental work and for sharing their previous research outputs, as a reference for this dissertation.

To my fellow colleague, Pedro Castro, I would like to thank you for all the advice and patience.

As honorable mentions I would like to thank my friends and fellow colleagues from my academic course, Sofia and Ana, for their friendship and shared advice.

Table of Contents

List of Figures

List of Tables

List of abbreviations

3D: 3 (three) dimensional

ATR-FT-IR: Attenuated Total Reflection Fourier-Transform Infrared

BNC: Bacterial Nanocellulose

CNC: Cellulose Nanocrystals

CNF: Cellulose Nanofibers

MAPLE: Matrix Assisted Pulsed Laser Evaporation

MONPs: Metal Oxide Nanoparticles

MRI: Magnetic Resonance Imaging

MTS: 3-(4,5-dimethylthiazol-2-yl)-5-(3-carboxymethoxyphenyl)-2-(4-sulfophenyl)-2H-tetrazolium

MTT: 3-(4,5-dimethylthiazol-2-yl)-2,5-diphenyl-2H-tetrazolium bromide

PXRD: Powder X-ray Diffraction

SEM: Scanning Electron Microscopy

SPP: Solid-Phase Peptide

TAPPI: Technical Association of the Pulp and Paper Industry

TEM: Transmission Electron Microscopy

TEMPO: 2,2,6,6-Tetramethylpiperidine-1-oxyl

UV: Ultraviolet

UV-Vis: Ultraviolet-Visible

Scientific outputs

Papers

Miranda C, A. Silva J, L. Ramos O, Castro P, E. Pintado M, Pereira CF. *Cellulose Nanocrystal–ZnO Nanohybrids as Wound Healing Potentiators.* [Manuscript in preparation]

Miranda C, A. Silva J, L. Ramos O, E. Pintado M, Pereira CF. *Hybrid-Based Wound Dressings: Combination of Metal Oxides and Biopolymers.* [Manuscript in preparation]

Poster Communication

Miranda C, A. Silva J, Capela D, Lopes T, L. Ramos O, E. Pintado M, Silva A. N., Pereira CF. *Cellulose Nanocrystal-ZnO hybrid systems: Design, Characterization and ZnO quantification with LIBS technology*. Poster presented in Simposio EMSLIBS 2023, Porto, 4th September 2023

1. Introduction

1.1. Hybrid nanomaterials: General Considerations

Hybrid nanomaterials are constituted by the conjugation of two or more components at a nanometer scale. These materials can have both inorganic and organic building units, functioning as an organic-inorganic hybrid system.[1] By conjugating two or more components, it is possible to combine the intrinsic characteristics of each and have a synergistic effect with the introduction of interesting properties such as biocompatibility, biodegradability, transparency, high mechanical stability, antimicrobial activity, sustainability, among others, which are desirable traits for wound healing, drug delivery, medical imaging and other applications.[2–6]

Among the hybrid nanomaterials, there is an increasing interest on the cellulose-based nanomaterials, particularly nanocellulose and metal oxide nanoparticles hybrids, as confirmed by the increasing number of publications (Figure 1). The Figure 1 shows accounts for all published research papers with nanocellulose and metal oxides as keywords query search. Thus far, there is a total of 155 published scientific papers pertaining to keywords query search with nanocellulose and metal oxides as topics, and about half of these were published in the last 3 years. Of those 155 papers, 21 include nanocellulose and zinc oxide as main topics from the period between 2017-2023, at the time of the search.

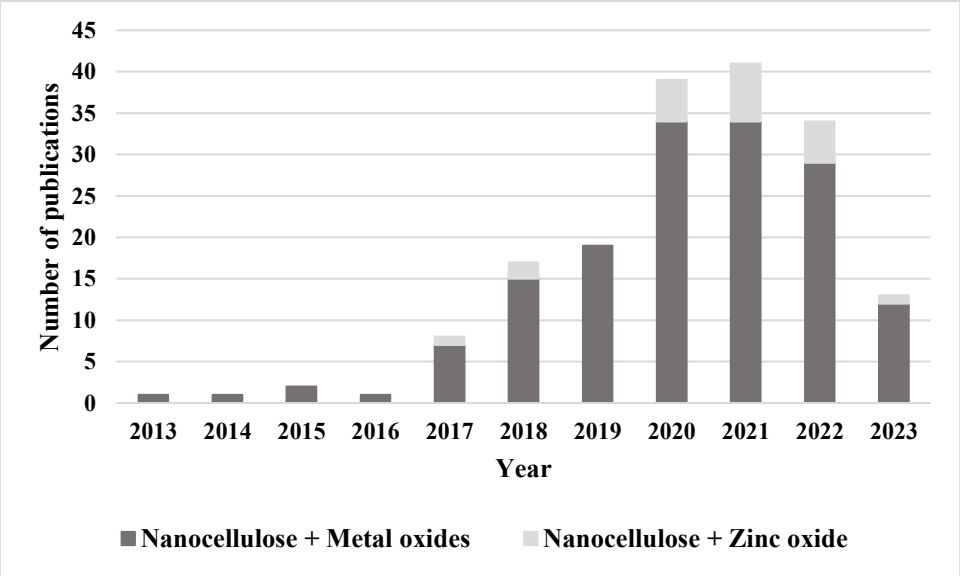

Figure 1. Number of publications on topics of nanocellulose and metal oxides, as well as nanocellulose and zinc oxide, from 2013 to 2023 using Web of Science™ platform.[7]

Pertaining the scientific publications illustrated in Figure 1, a significant number of applications for hybrid materials comprising of nanocellulose and metal oxides has been explored: food packaging,[8,9] material reinforcement,[3,10–12] wastewater treatment,[3,13] antimicrobial materials,[14–16] wound healing,[17,18] among others.

The commercialization of hybrid materials comprising nanocellulose and metal oxides implies the process scalability at low cost, with low environmental impact, and low toxicity. However, research so far has only produced hybrids at a laboratory scale. In addition, studies on environmental toxicity are at an early stage for nanocellulose-based hybrids, further delaying their entry into the market. When combining metal oxides with nanocellulose matrix, the agglomeration tendency of metal oxides is a challenge in the preparation and processing of the hybrids due to negative effects that may compromise the materials' desired properties. For wound healing applications, a simultaneous balance between increased flexibility, toughness, and antimicrobial activity of materials has been a challenge in terms of materials design. With the increase in metal oxides concentration, there is an increase in antimicrobial activity and other functionalities; however, the toxicity of the hybrid also increases, and an equilibrium needs to be established.[3,12]

1.1.1. Construction Building Units

1.1.1.1. Nanocellulose

Cellulose is a renewable, sustainable, and affordable resource, and, on a nanometer scale is referred to as nanocellulose. It can be obtained from plants, algae, wood, and other organic sources by chemical treatments that remove lignin, hemicelluloses and other impurities as waxes.[12]

This organic compound is formed by β-1,4-linked glucopyranose units, and each unit is associated to three hydroxyl groups, which yield the high hydrophilicity and biodegradability of the compound. Cellulose construction units have a polymerization degree that ranges from hundreds to thousands of units. They are packed into microfibrils, which are structures comprised of construction units disposed in orthogonal layers. On the other hand, microfibrils are stabilized by hemicellulose and lignin that are connected via hydrogen bonds and intermolecular electrostatic forces, namely, van der Waals forces.[12,19]

Figure 2 shows a schematic representation of cellulose structure and illustrates the various levels of complexity from the lowest (β-1,4-linked glucopyranose units) up to the highest with their integration within the cell wall.

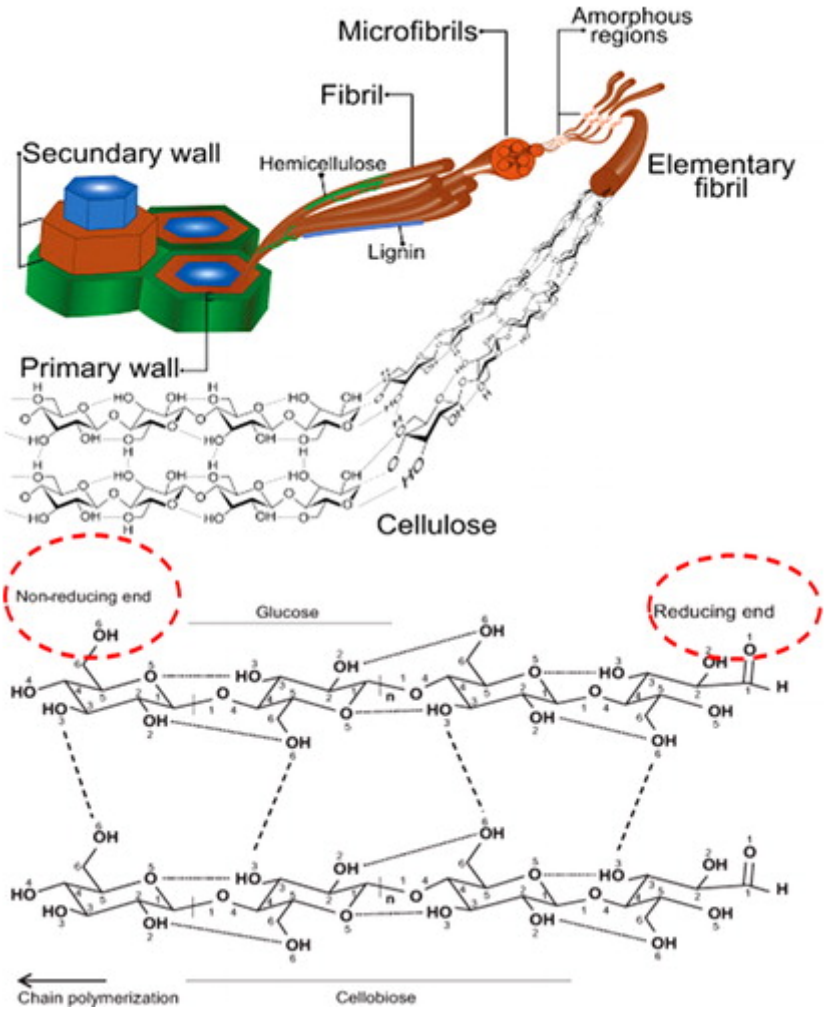

Figure 2. The structural arrangement of cellulose. Image adapted from Oun *et al.* (2020).[3]

Nanocellulose is isolated from cellulose sources by mechanical disintegration (e.g., high-power ultrasonication) or by chemical treatments, namely acid and basic hydrolyses. Mechanical disintegrations can be preceded by chemical or enzymatic pre-treatments to reduce the energy needed for defibrillation. Tetramethylpiperidine N-Oxyl (TEMPO)-oxidation is a usual pre-treatment used in this case that allows easier defibrillation and functionalization of cellulose, with the introduction of carboxyl and aldehyde groups to the surface of the compound.[12,20]

Several terminologies have been used for cellulosic materials, particularly for materials with similar crystallinity, size, and shape characteristics. The use of several terms for one object may lead to ambiguities and misunderstandings due to nomenclature issues, as is the case of cellulose nanocrystals being also denominated as cellulose nanowhiskers, nanocrystalline cellulose, cellulose nanorods, among others.[21–25]

Considering the nomenclature issues on cellulosic materials, there have also been some anomalies concerning their classification in current literature.[24,26] In the review

article from Trache *et al.* (2020), the authors consider their division into two major classes: a) nanostructured materials that include cellulose microcrystals and microfibrils and b) nanofibers that include, in turn, nanocellulose with three different classifications, which differ according to morphology, size and extraction method- cellulose nanocrystals, cellulose nanofibrils and bacterial cellulose. This classification of nanocellulose materials was established by a draft version standard from Technical Association of the Pulp and Paper Industry (TAPPI) designated as TAPPI WI 3021: Standard Terms and Their Definition or ISO/TS 20477:2017.[27,28] This nomenclature standard and classification of cellulosic materials is also adopted in other recent literature reports such as the ones from Gorbunova *et al.* (2023) and Barhoum *et al.* (2022).[21,29]

Below, Figure 3 presents the different hierarchical structures of cellulosic materials divided according to the aforementioned standard.

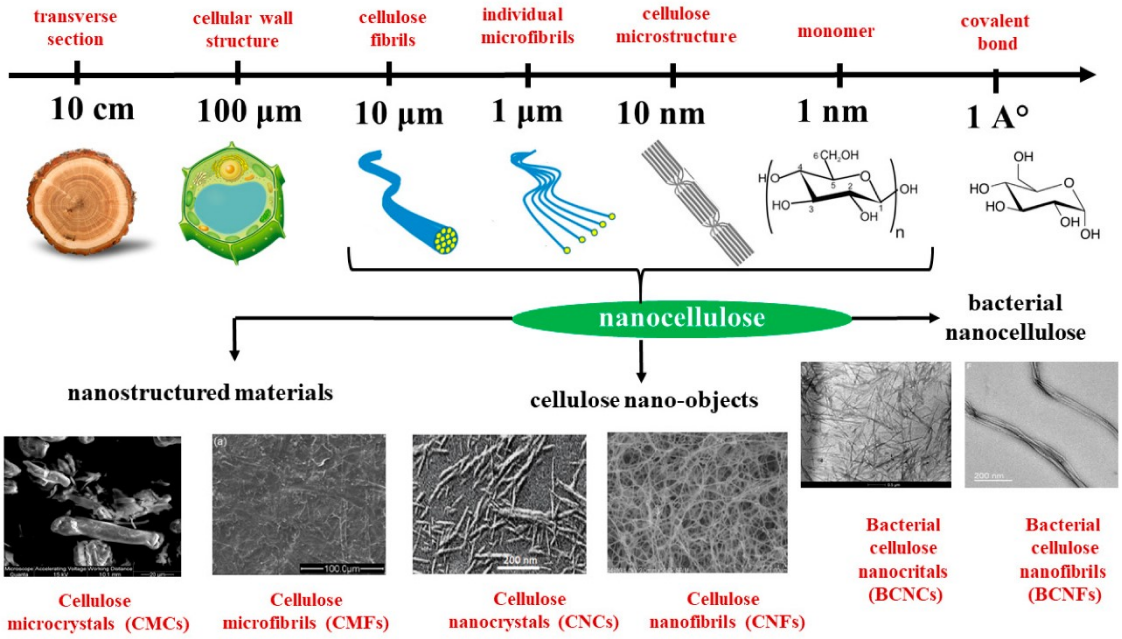

Figure 3. Hierarchical structures of cellulosic materials and their classification according to the TAPPI standard (ISO/TS 20477:2017). Image taken from Gorbunova *et al.* (2023).[29]

Cellulosic materials are divided into two major classes according to their shape and size. In this work, there will be a focus on nanocellulose as cellulose nano-objects, and their nomenclature will follow the one employed by the TAPPI standard from ISO/TS 20477:2017.[28]

Nanocellulose structure and properties vary with the method of extraction. When the main technique applied is a mechanical treatment, nanocellulose is commonly present as cellulose nanofibrils (CNF). On the other hand, when nanocellulose is obtained, for example, by acid hydrolysis, cellulose nanocrystals (CNC) are obtained. Additionally, nanocellulose can be obtained via bacteria or other microbial synthesis and, in this case, is designated as bacterial cellulose (BNC).[12,20,22,30]

Below in Figure 4, it is represented the different morphologies of nanocellulose by Electronic Microscopy (Transmission Electron Microscopy (TEM) and Scanning Electron Microscopy (SEM)).

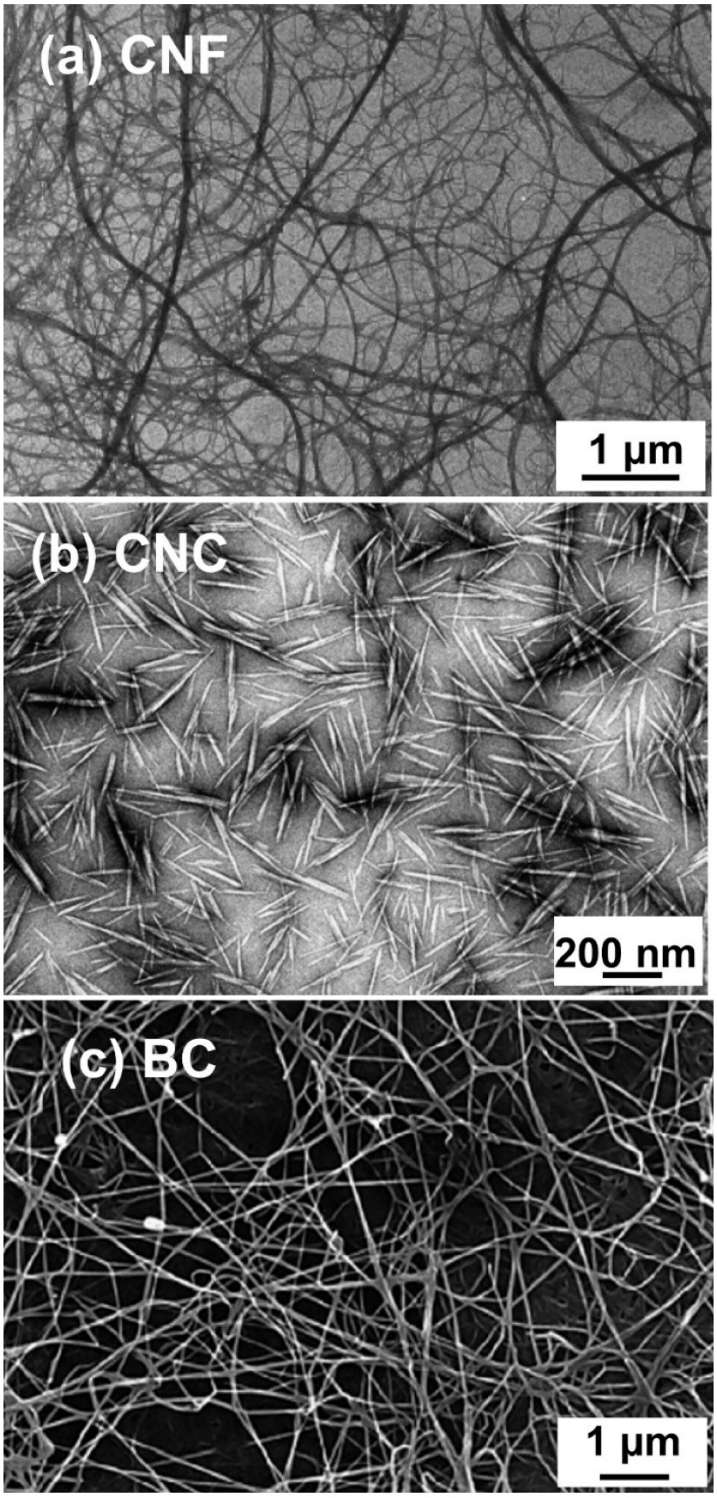

Figure 4. TEM (a, b) and SEM (c) images of the different types of nanocellulose, illustrative of their typical morphology: (a) cellulose nanofibers, CNF; (b) cellulose nanocrystals, CNC and (c) bacterial nanocellulose, BC. Image adapted from Solhi *et al.* (2023).[22]

Due to the more conservative isolation method, CNFs contain more amorphous regions compared to CNCs since the fibrous structure of the former is conserved (Figure

4). In acid hydrolysis, these regions suffer disintegration, giving nanocellulose the characteristic rod-like and higher crystallinity index.[12,20,22,30] According to Solhi *et al.* (2023), BNC is similar to CNFs due to possessing semicrystalline fibers (Figure 4), although their cross-sectional disposition is different and akin to rectangular form.[22] Commercially, nanocellulose can be obtained in the form of CNFs and CNCs. It is possible to obtain CNCs through CNFs but not the reverse, with a combination of mechanical disintegration and chemical treatment.[31]

According to TAPPI standard classification, nanocellulose materials are classified according to aspect ratio (length/diameter), diameter and length: diameter between 5-30 nm and a length between 100-600 nm for CNFs with an aspect ratio greater than 50; diameter around 3-10 nm and an average length inferior to 500 nm for CNCs and an aspect ratio greater than 5, and BNC is considered to have a diameter between 10-40 nm, length superior to 1000 nm (micrometer scale) and possessing an aspect ratio from 100 to 150.[28,29]

However, these dimensions are simply a recommendation for their classification. Recent literature also reported CNFs as having an average length in the micrometer scale between 1-15 μm and CNCs also reaching lengths in the micrometer scale, ranging between 50 nm to 10 μm.[22]

The crystallinity is an important parameter to be evaluated since it will impact many physicochemical properties. It can be afforded by X-Ray Diffraction, namely by Powder X-Ray Diffraction (PXRD) analysis, and it varies in the nanocellulose materials according to the cellulose source and isolation method. Current literature reports have identified CNCs with a crystallinity index between 58 to 90% and BNC with 80 to 100 %, depending on the material source.[29,32]

Nanocellulose-based materials have been widely used for material reinforcement, biomedical applications, and in the electronics field (due to inherent high thermal conductivity), as reported by Oun *et al.* (2020).[3]

Despite having some desired properties such as biocompatibility, biodegradability, and high stiffness for material reinforcement, nanocellulose lacks some properties that metal oxide nanoparticles have, such as antibacterial, optical, magnetic, and special electronic properties.[12,20,33]

1.1.1.2. Metal Oxides

In line with what was aforementioned, metal oxides are relevant as construction units of hybrid materials due to their properties and desirable traits such as bandgap, low toxicity, high thermal and chemical stability, electron conductivity, increase of surface area, and due to being economically accessible.[34,35] The properties of the metal oxide nanoparticles depend on the synthesis method and conditions applied. The combination of nanocellulose with metal oxide nanoparticles allows for the acquisition of new and enhanced properties. Also, nanocellulose can be used as a supporting material in their production to improve the dispersion of these nanoparticles. [3,12]

Many metal oxide nanoparticles are described in the literature to attain hybrid materials with nanocellulose, including, but not limited to ZnO, TiO_2, MgO, CuO, and Fe_3O_4 nanoparticles.[12,35–38]

In the last decade, ZnO, CuO and Ag nanoparticles were considered the most attractive due to their potential applications in electronics, polymers, biosensors, ceramics, inks, biocides, biomedical products, among other fields. These nanoparticles have been gaining interest in potential biomedical applications and food packaging studies due to their antibacterial and UV barrier properties.[3,18,39–41]

Amongst metal oxide nanoparticles, zinc oxide nanoparticles seem to have a promising potential for application in wound healing, with literature reporting these nanoparticles embedded in nanocellulose as displaying significant antibacterial properties, whereas, amidst photocatalytic inorganic materials, zinc oxide nanoparticles showed high efficiency with photo-induced oxidation and the consequent production of reactive oxygen species. Zinc oxide is also considered a safe material according to the Food and Drug Administration.[3,12,16,35]

Zinc oxide nanoparticles may be obtained through two different synthetic approaches: synthesis *via ex-situ* or *in-situ* methods. In the *ex-situ* approach, these nanoparticles are synthesized separately and later added to a polymeric matrix. They can be deposited onto polymers *via* physical means, such as electrospinning and melt-spinning, or *via* chemical means, as is the case of immersion of polymer in solution or dispersion containing the metal nanoparticles[42]. In the *in-situ* preparation methods**,** the polymeric matrix, in this particular case, nanocellulose, exhibits a double function as a template and a reducing agent in the obtention of the zinc oxide nanoparticles.[12]

In general, *in-situ* methods allow for a good spatial distribution of zinc oxide particles within the polymeric matrix and better dispersion, preventing agglomeration, with the main disadvantage relying in the influence of unreacted groups from the polymeric base on the final product´s properties. On the other hand, the *ex-situ* methods possess, as the critical factor, the lack of appropriate dispersion of the zinc oxide particles onto the polymeric matrix, but allow the possibility of larger scale production .[43]

The selection of the synthetic approach to attain ZnO nanoparticles will be largely influenced by the intended application and/or desired characteristics, such as size and morphology.[44,45] Conventional synthesis approaches include: hydro/solvothermal synthesis; sol-gel synthesis; synthesis by controlled precipitation and by chemical vapor deposition.

Hydrothermal synthesis (Figure 5), which constitutes an environmentally-friendly process due to not requiring any organic solvents or additional processing such as calcination, for example. It can be performed at high temperatures, usually at a range from 80 to 250 ºC, and high pressure environment (e.g., autoclave), and the resulting product may have a wide variety of shapes and dimensions, presenting high purity and crystallinity. Solvothermal synthesis is a similar process, but the solvent used is any other than water (ethanol, for example). The main disadvantage for hydrothermal/solvothermal method is the requirement for expensive equipment and high temperatures.[44,45]

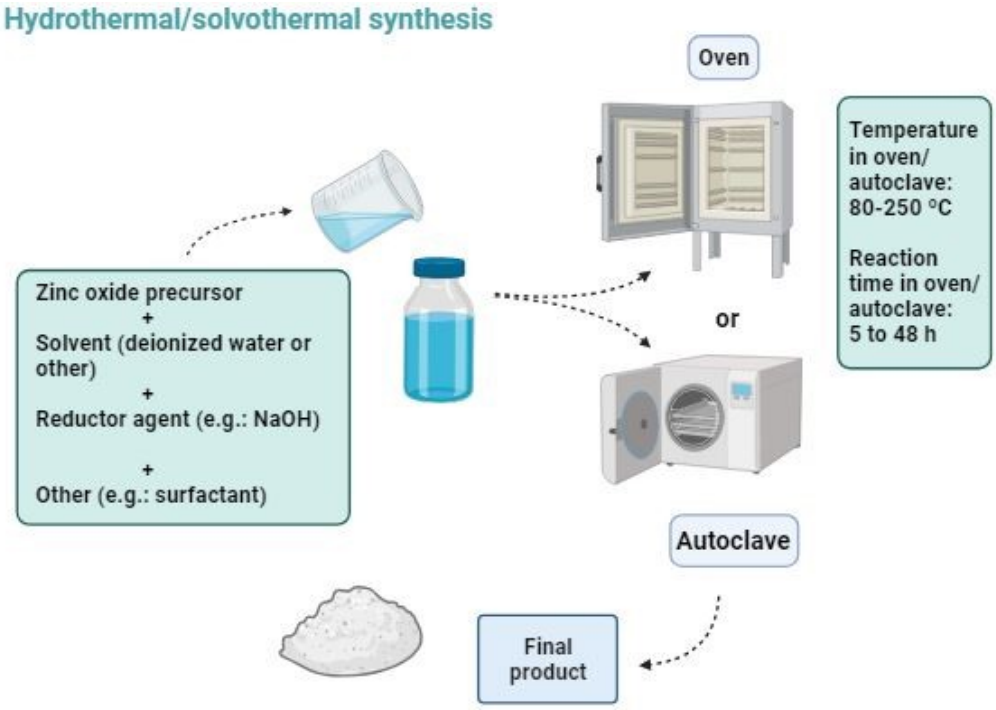

Figure 5. Schematic representation of hydrothermal synthesis for ZnO particles.[44,45]

Sol-gel synthesis (Figure 6) is a widely applied method due to its reliability, repeatability, low cost, and simple execution. ZnO obtained from this method presents favorable optical properties. However, the cost of raw materials may be steep and oftentimes volume shrinkage occurs, as well as cracking during the drying process.[44,46]

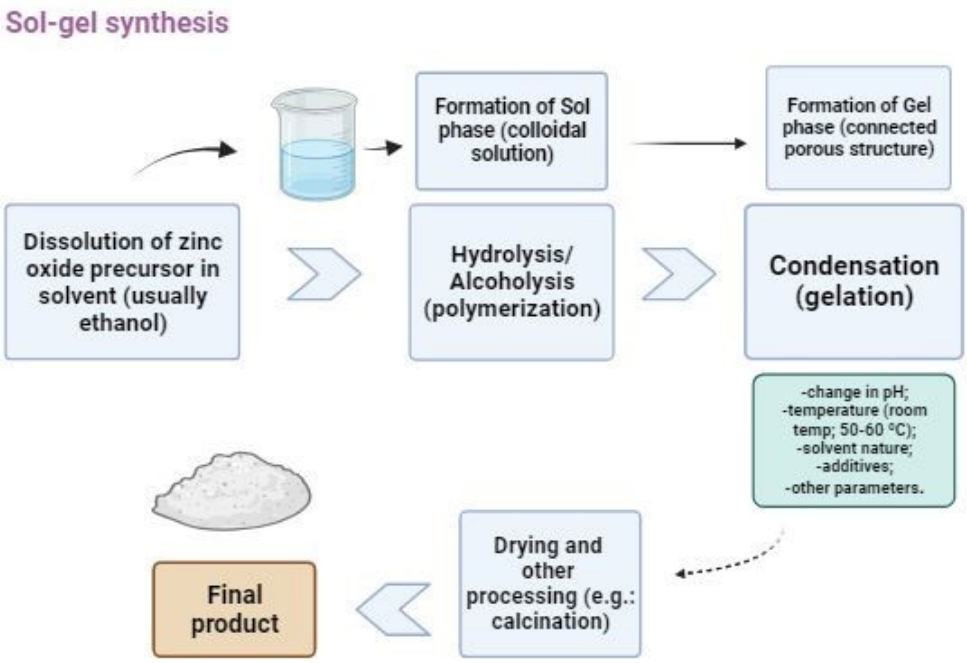

Figure 6. Schematic representation of sol-gel synthesis with the main stages for obtaining ZnO particles.[44,47]

Controlled precipitation (Figure 7) allows the production of ZnO with reproducible properties, such as dimension sizes. The main disadvantage would be the difficulty in breaking down the agglomerates formed during the precipitation of the precursor.[44,45]

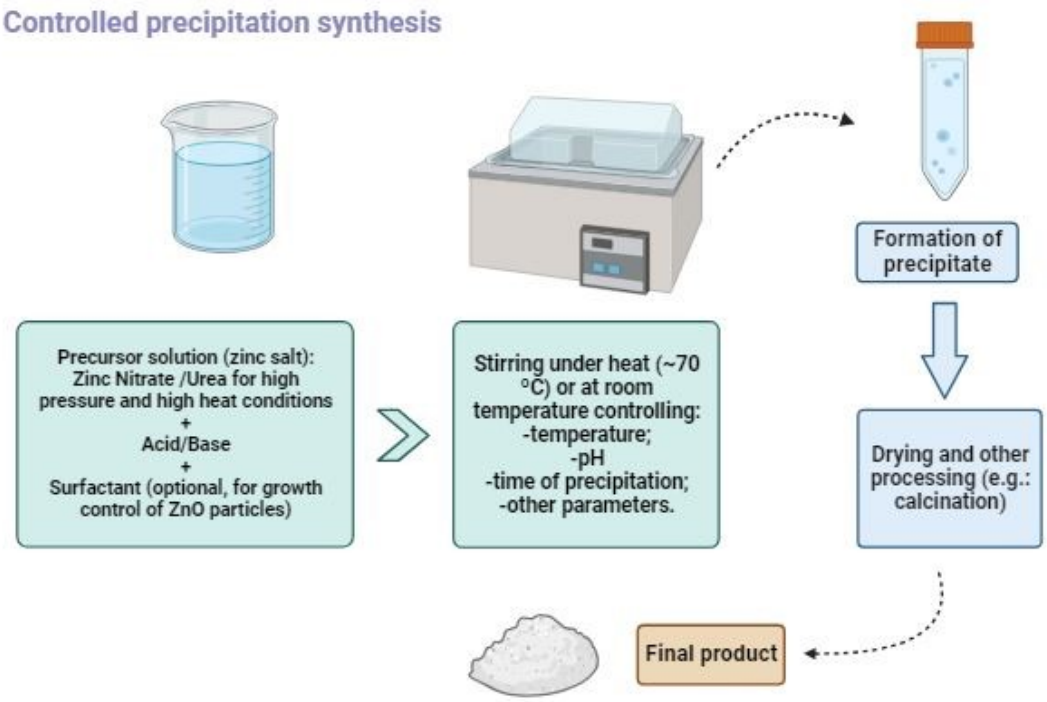

Figure 7. Schematic representation of controlled precipitation synthesis for ZnO particles.[44,45]

Chemical vapor deposition (Figure 8), where gaseous substances react with the substrate. Chemical vapor deposition is preferred for uniform film coating with high purity, low porosity, and high stability. A main disadvantage of chemical vapor production of ZnO particles is the formation of toxic by-products. [45,48,49]

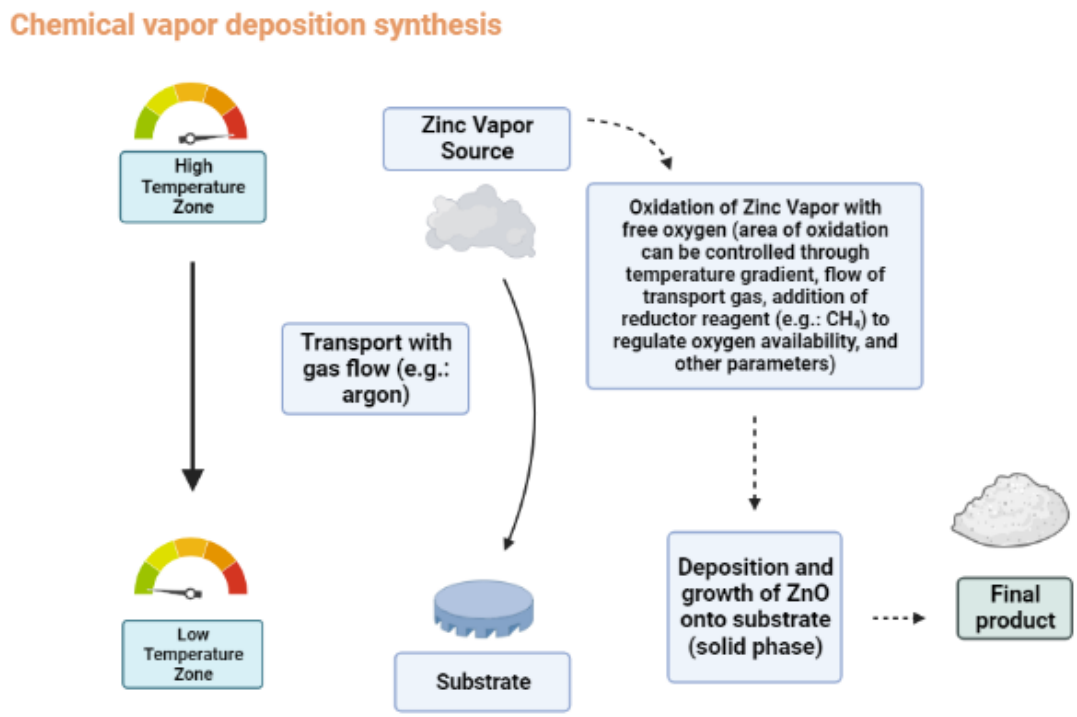

Figure 8. Schematic representation of chemical vapor deposition synthesis for obtaining ZnO particles.[45,50]

Apart from the synthetic approaches described, there are physical synthesis approaches that may require higher temperatures, like thermal evaporation approach, or high-energy milling, as is the case of the mechanochemical process, and they are preferred for industrial-scale production. However, obtained products have a lower purity, and parameters such as size and morphology are harder to control.[44,45,51,52]

In recent literature, efforts have been observed in developing greener alternatives for the synthesis of ZnO particles by adopting plant-based or microorganism-based approaches, sonochemical methods, amongst others, for a more economical and/or environmentally friendly process.[44,45,53,54]

1.1.2. Synthetic approaches applied to Nanocellulose/Metal Oxides hybrid materials

Generally, chemical synthetic approaches have been preferred over physical ones due to the requirement of simpler equipment, the utilization of milder reaction conditions, and the ease of scale-up.[35]

Recently, conventional synthetic approaches of nanocellulose/metal oxides hybrids that were most employed include: sol-gel,[55–57] sonochemical, [37,57] hydrothermal, [55,57,58] co-precipitation, [37,59,60] and microemulsion [37,55,57].

For dispersion and growth of metal oxide nanoparticles (MONPs) within nanocellulose, some interactions must occur regardless of the synthetic approach applied (*ex-situ* or *in-situ*).

In-situ growth of MONPs is possible without any external reducing or capping agents (which may be introduced through surface modification, as is the case of TEMPO-mediated oxidation, for example). Cellulose without surface modification binds and stabilizes MONPs through ion-dipole interactions via surface hydroxyl groups and MONPs are generated through nucleophilic interactions. Surface hydroxyl groups can be activated using hydrothermal synthesis, UV, and microwave irradiation methods.[3]

The addition of negatively charged groups via surface modification allows for better dispersion of MONPs and better colloidal stability due to electrostatic repulsion. Some common forms of surface modification on cellulose include sulfonation, *via* hydrolysis with sulfuric acid, and carboxylation by TEMPO-mediated oxidation. Non-covalent surface modification is possible with the adsorption of surfactants, interacting with cellulose surface *via* hydrogen bonds and van der Waals forces.[3]

1.1.2.1. Preparation of Nanocelluose/ZnO hybrid materials

A significant number of hybrid materials comprising nanocellulose and zinc oxide are reported in current literature. Table 1 summarizes this type of hybrids obtained through different synthetic approaches.

A great number of CNC and CNF-based hybrids reported in the literature (Table 1) have been synthesized through *in-situ* hydrothermal method.[58,61–63] One simple and possibly scalable synthesis method seems to be the *in-situ* solution casting approach, which allows the obtaining of small and well-dispersed zinc oxide nanoparticles.[64,65] BNC-based hybrids explore equally *ex-situ* and *in-situ* synthetic approaches.[66–72]

Ex-situ synthetic approaches commonly include immersion,[67] where nanocellulose is immersed in zinc oxide solution, deposition with surface spraying of nanocellulose[71] or other techniques such as MAPLE (matrix assisted pulsed laser evaporation) deposition [68] and mixing of zinc oxide solutions with nanocellulose solution[67,72,73]. Nanocellulose-based construction units have been functionalized using electrospinning deposition

method[58,63] and *via* a novel synthesis method of the nanohybrids: MAPLE deposition technique, with deposition of ZnO particles onto bacterial nanocellulose 3D matrix[68].

Some optimizations on *in-situ* synthesis methods have been achieved, such as the implementation of simpler protocols with two-step[62] and one-step[63] hydrothermal syntheses; synthesis processes assisted by sonication, allowing for preservation of nanocellulose 3D matrix[66] and green methods such as SPP (solid-phase peptide) synthesis, that bypasses the need for a reducing agent compared against a synthesis using ammonium hydroxide as reducing agent[69].

The simplest preparation methods in terms of time spent for hybrid synthesis took about 40 min to an hour[72–74], and the materials prepared were either freeze-dried[72,73] or had a short dry time, as is the case in Azizi *et al.* (2013)[74] with drying for 1 h at 120 °C.

Table 1. Overview of hybrid materials comprising nanocellulose and zinc oxide nanoparticles.

Nanocellulose-based construction units	Synthetic approach									Morphology of ZnO	Hybrid form	Potential application	Obs.	Ref.
	In situ/Ex situ	Method	Reaction Time	Temp. (°C)	Metal oxide precursor and/or zinc oxide unit	Solvent	Washing step	Drying	Other reagents					
CNF	*In situ*	Chemical bath deposition	>7 h	Stirring at 60 °C of zinc acetate dihydrate and NaOH solutions; Dipping of cellulose fibers on chemical bath at 4 °C (30 min) and drying at 100 °C (30 min); Stirring at 100 °C (6 h) for growth of ZnO particles	$Zn(CH_3CO_2)_2.2H_2O$;	Isopropanol and deionized water	Thorough wash with deionized water	Drying in hot air oven for 24h at 60 °C	NaOH; HMT (hexamethylenetetramine); $Zn(NO_3)_2.6H_2O$	Spherical and nanorod-shape like	Pellet	UV and humidity sensor	With increase of the surfactant (HMT), ZnO particles form smaller agglomerates	75
Modified CNF	*Ex situ*	Electrostatic assembly in aqueous medium with polyelectrolytes as macromolecular linkers	40 min	N.a.	ZnO colloid in commercial form (1% w/w in diethylene glycol) from Colorobbia (Italy)	NaCl and deionized water	Cellulose nanofibers were washed 2 times with deionized water after each mixing step with PDDA and PSS (6 washes total); Final wash with deionized water after mixing with ZnO colloid.	Freeze drying of sample suspensions for further characterizations	Polyelectrolytes: PDDA and PSS	"cauliflower-like" shape	Paper sheets	Production of antibacterial paper sheets with low content in ZnO	Authors denote a substantial production of reactive species of oxygen under light exposure conditions	73
CNF	*In situ*	*In situ* sol-gel synthesis	>10 h	Seeding of ZnO onto nanocellulose surface at 120 °C (pre-annealing); Annealing at 150-160 °C for 4 to 6 h; Growth of ZnO particles at 90 °C for 3 h	Zinc acetate	Ethanol and deionized water	2 washes with deionized water: one after annealing of seeded material and the other after growth of ZnO nanoparticles when immersed in chemical bath solution	90 °C for 5 min	HMT; $Zn(NO_3)_2.6H_2O$	Nanorods	Paper coating	Energy-harvesting devices (mechanical and thermal sources)	Authors were able to optimize synthesis method by employing a two-step protocol	62
Functionalized CNC	*In situ*	One-step *in situ* hydrothermal synthesis	> 24 h	Stirring of NaOH, $ZnCl_2$ and deionized water at room temp. (15 min); Reaction time in oven at 80 °C for 24 h	$ZnCl_2$	Deionized water	Several washes *via* centrifugation with deionized water and ethanol	60 °C for 12 h	NaOH; PEG; PHBV; DCM/DMF	Flower-like	Nanocomposite	Thermal energy storage and controllable drug release systems	Functionalization of novel phase change nanofibers *via* electrospinning	63
CNC	*In situ*	*In situ* hydrothermal synthesis	> 24 h	2 hydrothermal syntheses: a)heating of CNC and zinc nitrate hexahydrate mixture to 80 °C; b) hydrothermal growth in autoclave at 80 °C for 24 h of CNC and zinc chloride mixture	Zinc nitrate hexahydrate and zinc chloride	Deionized water	Washes via centrigugation (12 000 rpm at 10 °C, 20 min) with deionized water	N.a.	NaOH	Sheet-like; Flower-like; Spheroidal shape	Sheet	Absorption of cationic dyes	Different ZnO particle morphologies were observed at different pH (flower-like and sheet-like shape at higher pH and spheroidal-like shape at lower pH)	61

Table 1 (CONT.)														
Nanocellulose-based construction units	**Synthetic approach**									**Morphology of ZnO**	**Hybrid form**	**Potential application**	**Obs.**	**Ref.**
	In situ/Ex situ	**Method**	**Reaction Time**	**Temp. (°C)**	**Metal oxide precursor and/or zinc oxide unit**	**Solvent**	**Washing step**	**Drying**	**Other reagents**					
CNC	*In situ*	*In situ* sol-gel synthesis	> 1 h	Thermal stirring at 80 °C	Zinc acetate dihydrate	Deionized water	Several washes *via* centrifugation with deionized water	120 °C for 1 h	Ethanol and NaOH	Hexagonal shape	Nanocomposite	Antimicrobial material	Authors observed a stronger antibacterial activity of the nanohybrids against Gram-positive *Staphylococcus aureus* compared to Gram-Negative *Salmonella choleraesuis*	74
CNC	*In situ*	*In situ* solution casting	4 h	Magnetic stirring at 90 °C of zinc oxide precursor solution mixed with cellulose (1 h); Continuous stirring at 90 °C after white precipitate formation (3h).	Zinc acetate hexahydrate	Deionized water	4 washes with deionized water	Air drying overnight and subsequent drying at 65 °C in oven	NaOH	Irregular disc-like agglomerates	Nanocomposite	Antibacterial material and potential for wastewater treatment	Synthesis method employed is considered a cheap and simple approach and can potentially be performed on a industrial scale for wastewater treatment	65
CNC	*In situ*	One-step *in situ* hydrothermal synthesis	>24 h	Stirring at room temperature of NaOH and zinc chloride mixture; Storing of mixture after addition of CNC suspension at 80 °C for 24 h in oven	Zinc chloride	Deionized water	Washes by centrifugation with deionized water and ethanol	60 °C for 12 h	NaOH	Flower-like	Sheet	UV shielding against UVA and UVB irradiations and antibacterial activity	Study of effects of the obtained nanohybrid electrospun onto PHBV nanofiber	58
CNC	*In situ*	*In situ* solution casting	N.a.	Magnetic stirring at room temp. of aqueous solution with zinc oxide precursor and nanocellulose; Addition of ammonium hydroxide until pH=10 at 45 °C ; Overnight continuous stirring of the mixture at room temp.	Zinc nitrate hexahydrate	Deionized water	5 washes by centrifugation with deionized water and ethanol	80 °C for 6 h in oven	Ammonium hydroxide	N.a.	Paper coating	Antibacterial material	Synthesis method applied is inexpensive and allows the obtaining of small and well dispersed particles	70

Table 1 (CONT.)														
Nanocellulose-based construction units	**Synthetic approach**									**Morphology of ZnO**	**Hybrid form**	**Potential application**	**Obs.**	**Ref.**
	In situ/Ex situ	**Method**	**Reaction Time**	**Temp. (°C)**	**Metal oxide precursor and/or zinc oxide unit**	**Solvent**	**Washing step**	**Drying**	**Other reagents**					
TEMPO-oxidized CNF	*Ex situ*	Freeze-dried	N.a.	Heating at 70-80 °C until homogeneous slurry is obtained (containing nanocellulose and PEG solutions); After addition of ZnO, slurry is frozen at -20 °C	Zinc oxide nanopowder purchased in commercial form from Sigma Aldrich	Deionized water	None	Freeze-dried at -80 °C	Polyethylene glycol (PEG)	Agglomerates	Spongy	Topical bleeding	Wound dressing antibacterial material with significant potential to regulate topical bleeding and aid in the combat against bacterial infection, after infliction of traumatic dermal injury	76
BNC	*In situ*	Ultrasonic assisted *in situ* synthesis (sonochemical)	Up to 9 h	Stirring at 50 °C of zinc oxide precursor dissolved in water-ethanol solution	Zinc acetate dihydrate	Ethanol + Deionized water	Thorough wash with deionized water and sonication for 30 min	Freeze-dried	Ammonium hydroxide solution	"cauliflower fungus-like" shape	Sheet	Antibacterial wound dressing	Conservative synthesis method that preserves the 3D structure of BC matrix	66
BNC	*Ex situ*	*Ex situ* synthesis of ZnO by precipitation method, followed by immersion of nanocellulose membrane and mixing	> 24 h	Mixing of BC in ZnO suspension in shaking incubator at 50 °C, 150 rpm for 24 h, after immersion of BC membrane in ZnO suspension	Zinc nitrate tetrahydrate	Deionized water	None	Freeze-dried at -50 °C for 10 h	NaOH	Spheroidal	Nanocomposite	Wound dressing material	Nanocomposite showed enhanced wound healing and tissue regeneration compared to BC alone in animal burn model	67
BNC	*Ex situ*	MAPLE deposition technique	N.a.	N.a. (vacuum chamber)	Zinc acetate	Water; Chloroform	N.a. (sterilized by UV radiation)	N.a.	Ammonia	Agglomerates	Film	Antibacterial material	Novel synthesis method that allows the controlling of interfaces: matrix assisted pulsed laser evaporation (MAPLE) used for deposition of ZnO particles onto 3D matrix of BC	68
BNC	*In situ*	SPP synthesis and deposition of ZnO into nanocellulose pellicles	N.a.	Immersion of BC pellicles in aqueous solutions containing zinc ions at room temp.	Zinc nitrate hexahydrate; Zinc acetate dihydrate	Deionized water; Methanol	Sonication using deionized water (30 min)	Freeze-dried	Ammonium hydroxide	Plate-like and rod shaped	Pellicle	Antibacterial wound dressing and wastewater treatment	Authors consider the SPP synthesis method as a green technique, that bypasses the need for a reducing agent	69

Table 1 (CONT-)														
Nanocellulose-based construction units	**Synthetic approach**									**Morphology of ZnO**	**Hybrid form**	**Potential application**	**Obs.**	**Ref.**
	In situ/Ex situ	**Method**	**Reaction Time**	**Temp. (°C)**	**Metal oxide precursor and/or zinc oxide unit**	**Solvent**	**Washing step**	**Drying**	**Other reagents**					
BNC	*In situ*	Facile synthesis-impregnation of nanocellulose in ZnO precursor	> 34 h	After immersion of BC pellicles in solutions of ZnO precursor, mixture is shaken at 120 rpm, 24 h at room temp. Following placement in NaOH solution, seeded material is shaken in same conditions for 10 h	Zinc nitrate hexahydrate	Deionized water	Washed with deionized water	Vacuum-dried at 80 °C for 20 min by sheet former; Room temp. drying (6 days)	NaOH	N.a.	Film	Food packaging, wound healing and other biomedical applications	Functional hybrid with UV shielding, photocatalytic activity and antibacterial activity as properties	70
BNC	*Ex situ* + *In situ*	*Ex situ* synthesis of ZnO by sonochemical and sol-gel method; BC-ZnO nanocomposites were obtained *via* two different methods: surface spraying of BC films with ZnO aqueous solution and immersion of BC film in aqueous solution of ZnO precursor	N.a.	In one of the hybrid synthesis, namely with immersion of BC in zinc nitrate tetrahydrate, the seeded material is placed in NaOH solution for 10 min at 50 °C	Zinc acetate dihydrate; Zinc nitrate tetrahydrate	Ethanol	Washed with deionized water until pH=7	Vacuum-dried	BDP; NaOH	N.a.	Nanocomposite	Wound healing	Authors used BDP (Betulin-3,28-diphosphate) to modify ZnO nanoparticles and studied its effects. *In vivo* experiments were carried out to study the effect and properties of synthesized nanohybrids relevant to wound healing	71
BNC	*Ex situ*	Mixing of ZnO nanoparticles into bacterial cellulose solution	> 1 h	N.a.	ZnO in nanopowder form prepared from precipitation synthesis	NMMO; Deionized water	Washed with deionized water for 48 h	Freeze-dried	NaOH	Oval shape	Film	Development of nanocomposite with enhanced properties: regenerated BC with enhanced thermal, mechanical and bactericidal properties	Nanohybrid was obtained through a economically friendly method and displayed non-toxicity as well as significant cellular biocompatibility towards animal cells	72

Legend: CNF- cellulose nanofibers; CNC- cellulose nanocrystals, BNC- bacterial nanocellulose.

Synthesis methods that took longer than 24 h, such as the ones in Wahid *et al.* (2019), Khalid *et al.* (2017), and Abdalkarim *et al.* (2018), for example, are less economically friendly due to the time and resources spent - 24 h at 80 °C.[58,67,70]

A proposal mechanism to attain nanocellulose/ZnO hybrid materials *via in-situ* synthesis is depicted in Figure 9, based on the work developed by Wahid *et al.* (2019). They proposed the obtention of ZnO particles through adsorption of zinc ions on bacterial cellulose nanofibers with consequent conversion of those ions into ZnO by reaction with hydroxyl group. [70]

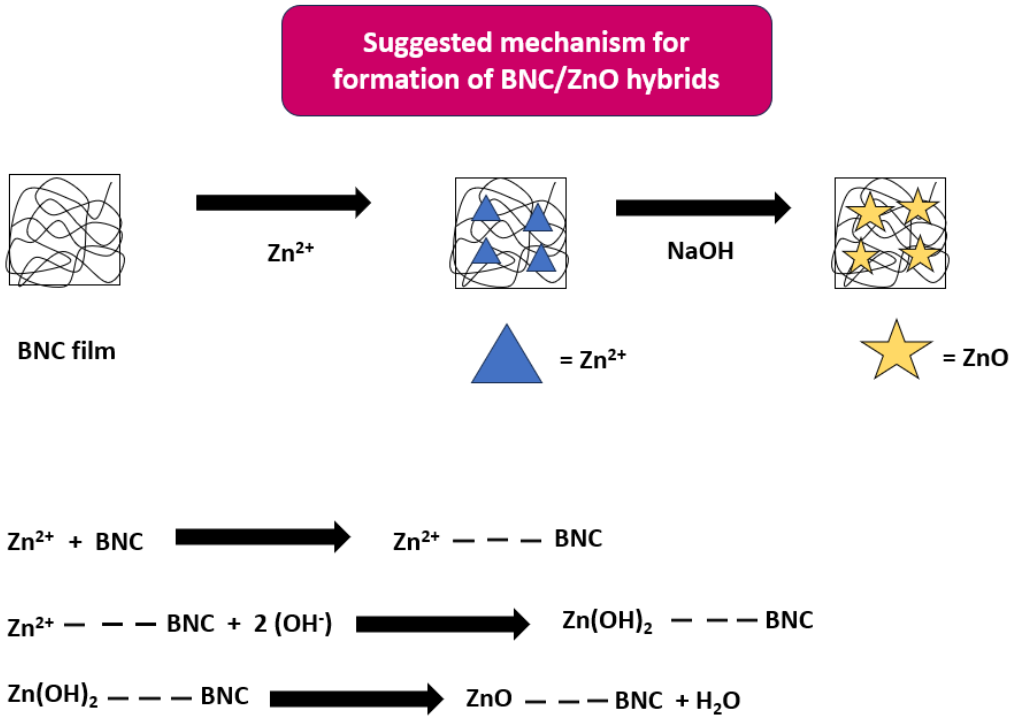

Figure 9. Proposal mechanism to attain a hybrid material of bacterial nanocellulose (BNC)/ZnO according to Wahid *et al.* (2019).[70]

This proposal is also supported by other literature reports, including other forms of nanocellulose in the hybrid compounds comprising similar construction units, namely CNC, BNC and zinc oxide.[66,69,74]

The zinc oxide particles of hybrid materials obtained by different *in-situ* and *ex-situ* synthetic approaches exhibited various morphologies: spheroidal/oval,[61,67,72,75] rod shape, [62,69,75] flower-like, [58,61,63,66,73] agglomerate shape, [68,76] sheet-like[61] and plate-like[69] structures that are depicted in Figure 9.

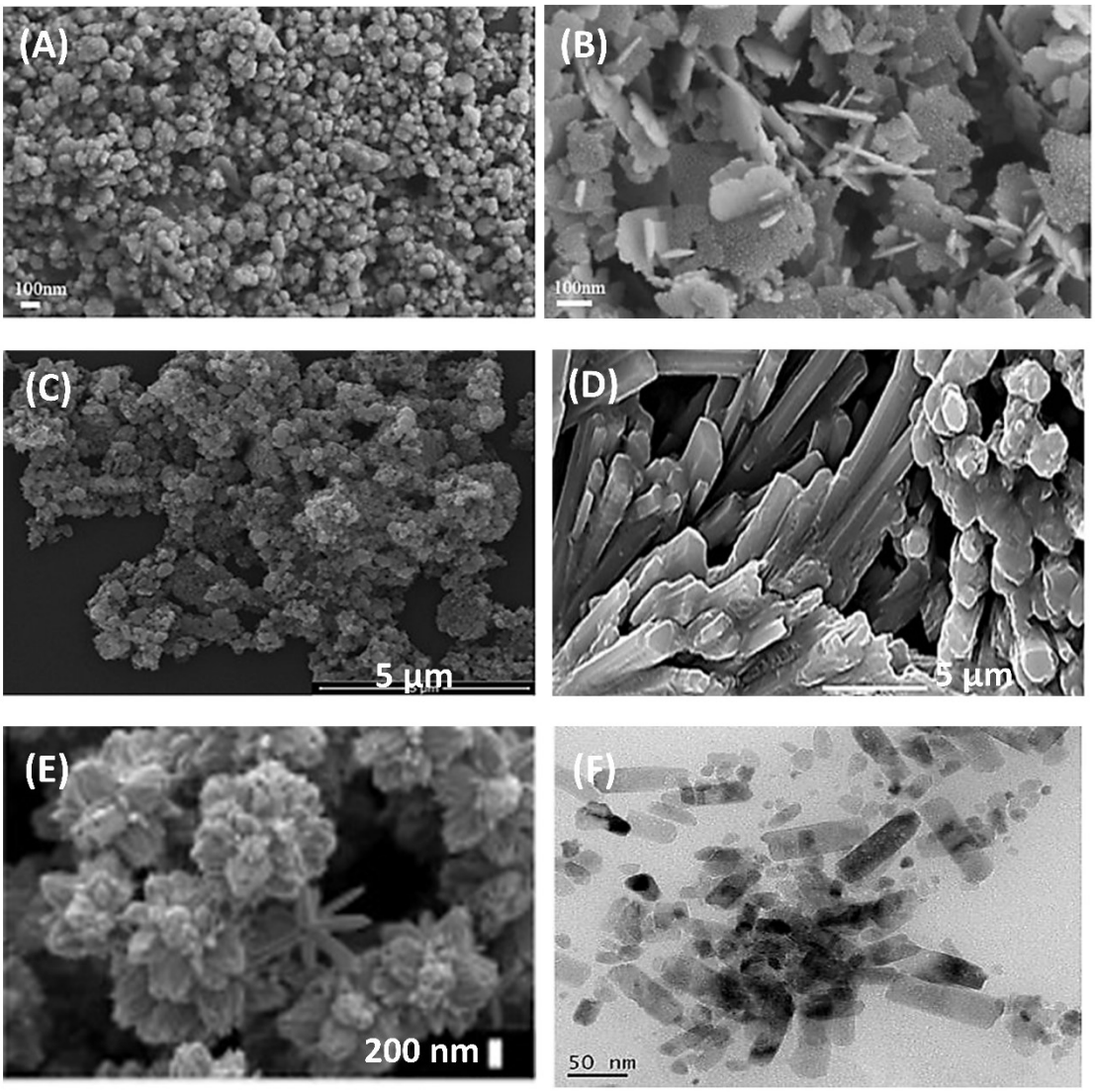

Figure 10. Morphologies of ZnO particles in hybrids composed of ZnO and nanocellulose: (A) spheroidal/oval[61]; (B) sheet-like[61]; (C) agglomerates[68]; (D) plate-like[69]; (E) flower-like[77]; (F) rod-like[75]. Images (A) to (E) were obtained *via* SEM microscopy, while image (F) was obtained through TEM microscopy.

Flower-like shape was commonly observed from *in-situ* hydrothermal syntheses,[58,61,63] and in the literature, a connection between the ZnO morphology and pH is established: formation of flower-like and sheet-like shapes at higher pH (11 and 10.5, respectively) and appearance of spheroidal shape in lower pH (8.5). As previously mentioned, a relation is established between the change in ZnO morphologies with the alteration of hydroxyl group content in the hybrids.[61]

The work reported by Wahyuono *et al.* (2016) describes a mechanism of ZnO nanoflowers obtention by wet chemical synthesis. At higher temperatures, dehydration reaction of $[Zn(OH)_4]^{2-}$ yields ZnO nuclei and extra hydroxyl groups, and, in low

hydroxyl group content, the nucleation rate is high. In conditions of low temperature for early growth phase of ZnO nuclei, the ZnO particles acquired hexagonal-ended nanorod morphology, while at higher temperatures and longer reaction times, ZnO acquired a prism-ended nanorod form. Nanoflower morphology is considered to be derived from the radial spatial arrangement of ten prism-ended nanorods (Figure 11).[77]

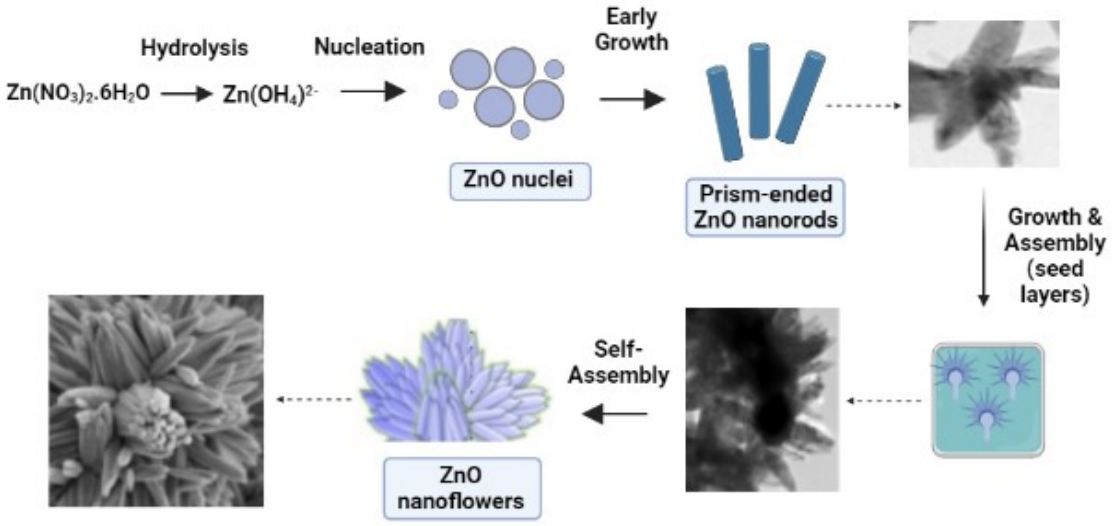

Figure 11. Schematic representation of the mechanism to obtain ZnO nanoflowers. Adapted from Wahyuono *et al.* (2016).[77]

1.1.3. Applications

The nanocellulose/metal oxide hybrids exhibit promising antimicrobial activity and significant enhancement over biofilms' properties such as thermal stability, UV-barrier, and mechanical properties.[3]

As an overview of the state of the art of the hybrid materials mentioned above, a summary pertaining different types of nanocellulose, metal oxide incorporated and their morphology, hybrid form, and potential applications related to the hybrid structure is highlighted in Table 2.

Table 2. Overview of the state of the art on nanocellulose/metal oxide hybrids.

Type of Nanocellulose	Metal oxide	Morphology	Hybrid Form	Potential application	Reference
CNC	Ag_2O	Spherical	Film	Antibacterial activity against *E.coli*	36
CNF	TiO_2	N.a.	Nanocomposite	Antibacterial activity against *E.coli, S.aureus*	38
CNF	CuO	N.a.	Freeze-dried nanofibrils	Antimicrobial activity against *C.albicans, S.aureus, E.coli*	78
CNC	Fe_3O_4	Spherical	Nanocomposite	Dual contrast agent for MRI scan	79
CNC	$CoFe_2O_4$	Spherical; Rod-like	"CNC-based dispersions, films and composite fibers"	Magnetically assisted drug delivery	80
CNC	ZnO	Spherulite	Sheet	Wound dressing	58
BNC	MgO	Spherical	Nanocomposite	Clinical wound healing	37
CNF	ZnO	Rod-like	Pellet	UV and humidity sensor	75
BNC	Fe_3O_4	Agglomerates	Hydrogel	Neuro-Endovascular Reconstruction	60
BNC	TiO_2	N.a.	Nanocomposite	Wound healing and tissue regeneration	15
BNC	CuO	Sheet-like	Film	Development of antibacterial materials	14
CNC	ZnO	Spherical, sheet and flower-like	Sheet	Absorption of cationic dyes	61

Legend: N.a.- not available.

From current literature reports, the most common applications described for hybrid nanomaterials comprising nanocellulose and metal oxides include (Figure 12): antibacterial or antimicrobial materials, which, in turn, exhibit a tremendous potential to

be used in food packaging and for wound dressing/healing purposes;[14,36,37,69,70,72,78] UV and humidity sensing;[75] wastewater treatment;[61,65,69] tissue regeneration;[15] neuro-endovascular reconstruction;[60] potential use as dual contrast agent for MRI (magnetic resonance imaging) scan or, in other words, potential use in medical imaging[79] and development of drug delivery systems.[63,80]

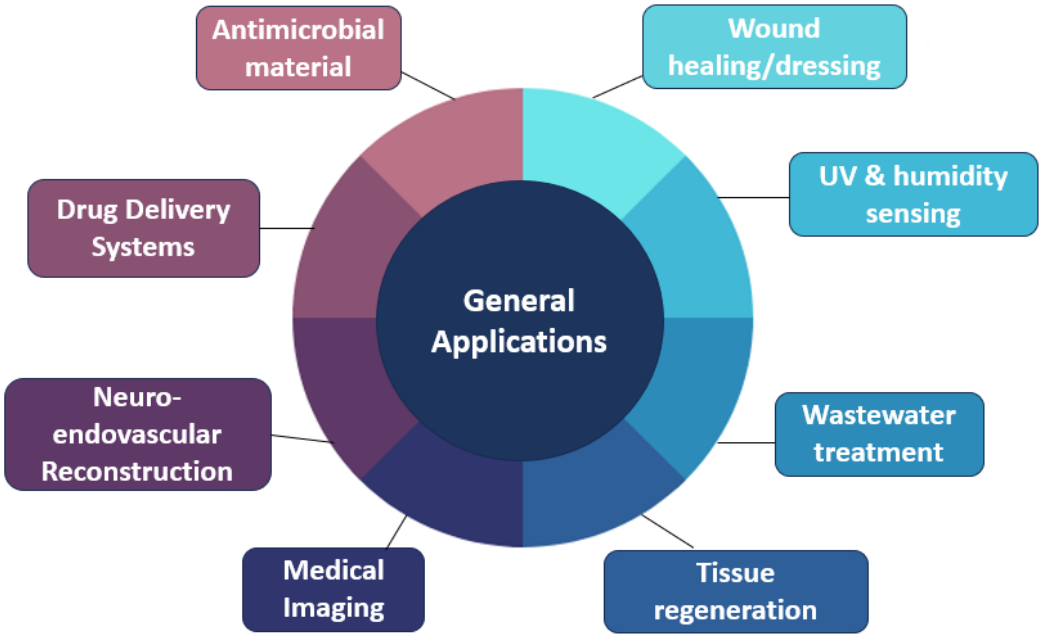

Figure 12. General applications of hybrids comprising nanocellulose and metal oxides.[14,15,72,75,78–80,36,37,60,61,63,65,69,70]

A special focus on hybrids composed of nanocellulose and ZnO will be given in this work owing to the fact that these type of hybrids are widely explored in materials science, engineering, food packaging and other areas, particularly due to possible use of these compounds as antibacterial agents, making for a great potential alternative to antibiotics, and, consequently, a possible solution to antibiotic resistance. [3,12,72,81]

As observed in Tables 1 and 2, hybrid materials comprising nanocellulose and zinc oxide have many potential applications (Figure 13), including: antimicrobial/antibacterial related purposes;[58,64–66,68,70,72–74] UV and humidity sensing;[75] UV shielding helpful for biomedical or cosmetic applications;[58] absorption of cationic dyes that may be useful for wastewater treatment;[61] energy-harvesting and storage systems;[62,63] sustained drug release systems[63] and regulation of topical bleeding[76].

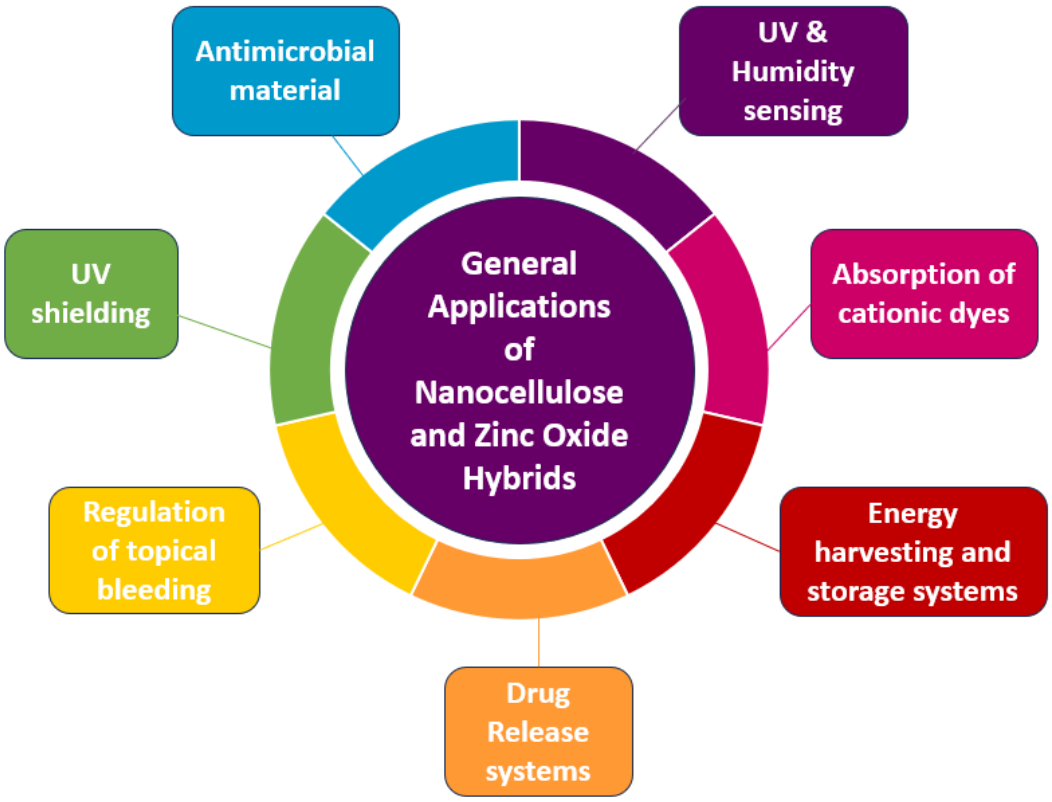

Figure 13. General applications of hybrids comprising nanocellulose and zinc oxide particles.[58,61–66,68,70,72–76]

The majority of hybrid materials comprising CNC or BNC and ZnO (Table 1) possess an antimicrobial/antibacterial activity.[64–66,68,72,74]

In the work developed by Trindade *et al.* (2013) was reported a hybrid material in paper sheet form comprising modified CNF and ZnO particles. This hybrid presented good antibacterial activity with a low content of ZnO.[73]

In this work there will be a focus on the applicability of nanocellulose-based/ZnO hybrids as wound healing/dressing materials. Some BNC-based/ZnO nanohybrids (Table 1) displayed great potential for the applicability mentioned above due to synergistic combination of bacterial nanocellulose and zinc oxide properties such as biocompatibility, low toxicity, and antibacterial effect on infected wounds. Their potential has been studied through *in vitro* and *in vivo* experiments (Figure 14), using animal cells and live animal models.[66–72,76]

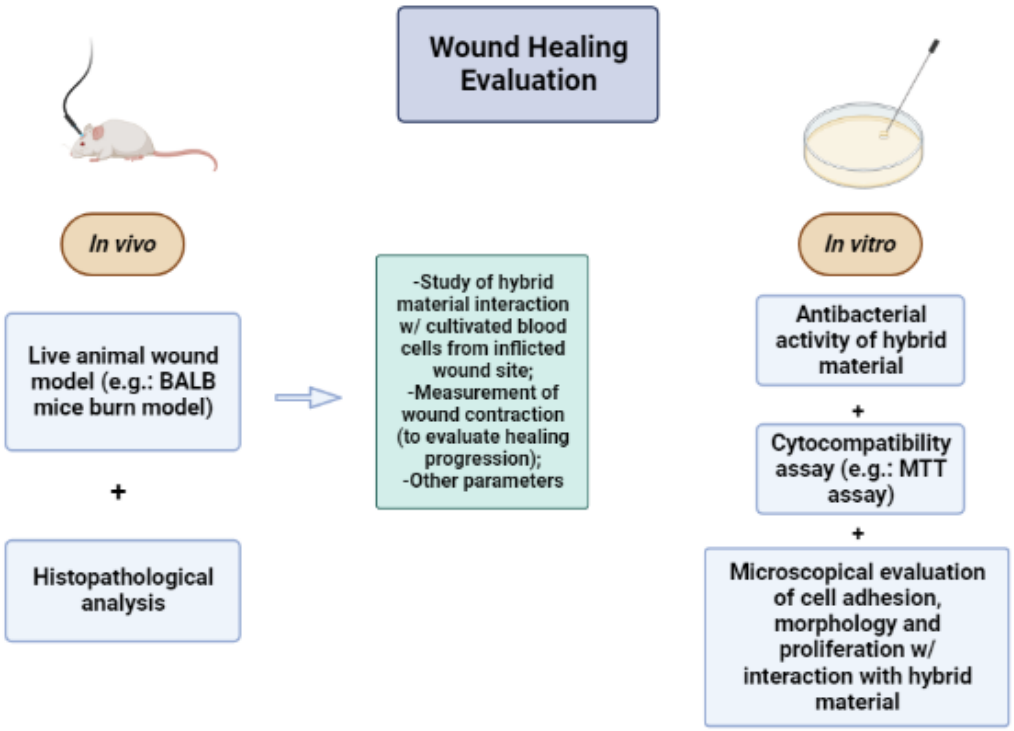

Figure 14. Most studied biological properties of nanocellulose/zinc oxide hybrids for wound healing/ dressing applications.[66–72,76]

Recent works that proposed wound healing applicabity for nanocellulose/ZnO hybrids equally explored *in vitro* assays for evaluation of antibacterial activity of obtained hybrids on common bacteria strains (e.g., *E.coli*).[68,70,72] Futhermore, cytocompability assays were carried out *via* 3-(4,5-dimethylthiazol-2-yl)-5-(3-carboxymethoxyphenyl)-2-(4-sulfophenyl)-2H-tetrazolium (MTS) method[68] and study of zinc release in water[72]. In the work of Ul-Islam *et al.* (2014), the interaction of prepared hybrid film with animal cells namely osteoblast cells from the MC3T3-E1 ATCC line was also evaluated.[72]

Works that suggested application of synthesized nanocellulose/ZnO hybrids as wound dressing materials mostly included *in vitro* assessment of antibacterial activity[58,66,67,69,76], and Shefa *et al.* (2019) and Melnikova *et al.* (2021) studied the cytocompatibility of obtained hybrids *via* 3-(4,5-dimethylthiazol-2-yl)-2,5-diphenyl-2H-tetrazolium bromide (MTT) assay using L929 fibroblast cell culture[71,76]. Some specific wound dressing applications have been studied, namely: hemostatic dressing for traumatic dermal injury with *in vivo* evaluation, particularly using rabbit ear arterial bleeding model in Shefa *et al.* (2019)[76] and burn wound dressing with histopatholgical analysis using sacrificed mice, and evaluation of healing progression using *in vivo* BALB mice burn model in Khalid *et al.* (2017) [67].

Besides nanocellulose/ZnO hybrids, other types of nanocellulose/metal oxides materials have been reported for wound dressing/healing. Here, are summarized some examples:

i) novel hybrids comprising of MgO and BNC synthesized by *ex-situ* and *in-situ* methods, where the authors suggest possible applications of the products obtained for clinical wound healing due mainly to hybrid antibacterial activity against *S.aureus* and *E.coli;*[37]

ii) hybrid nanocomposite comprising of regenerated BNC and TiO_2 nanoparticles obtained *via* simplified synthesis, with authors reporting biological properties like biocompatibility, non-toxic profile, and aid in cell proliferation, revealing potential for tissue regeneration and wound healing;[15]

iii) hybrids comprising BNC and Fe_3O_4 in hydrogel form, were explored as a potential alternative to conventional treatment, which consists mainly in procedures with invasive surgery, for aneurysms that cause brain injury. Mechanical properties of hybrids were studied using regular BNC and magnetic BNC, and both types displayed similar responses when compared against other samples from authors's previous work[82]. Significant cell viability and evaluated properties of the prepared hybrids displayed promising potential for neuro-vascular regeneration.[60]

The evaluation of the biocompatibility of the hybrid materials with animal cells is commonly performed by using the MTT assays.[15,71,76] For the evaluation of the antibacterial activity, the disc diffusion method seems to be the most common method in studies referring to antimicrobial and wound healing applications, commonly studying activity against *E.coli* and *S.aureus* bacteria.[37,66–70,72,76] In terms of nanocellulose type, hybrids comprising of BNC and any other metal oxide seem to have the most reports regarding wound healing/dressing applications, which may be due to enhanced biocompatibility derived from usually higher purity and the disposition of cellulose nanofibers.[15,37,60,66–72]

The application of nanocellulose/zinc oxide hybrid materials as wound dressing/healing materials demands further investigation to attain faster and cheaper synthetic processes easily scalable for their incorporation in the market, such as *in vivo* and *in vitro* studies for medium to long term exposure, other toxicity evaluations such as environmental toxicity and, lastly, clinical trials.[3,12,67]

1.1.4. Innovation and aim of this work

In this work, we intend to prepare hybrid materials comprising nanocellulose and zinc oxide nanoparticles through different *in-situ* synthetic approaches, perform their structural elucidation, and evaluate their potential for wound healing applications.

This task will be accomplished by the execution of the following specific goals:

i. Study the influence of different reaction parameters (e.g., ratio of reagents, temperature, and time) in the obtention of nanocellulose/ZnO hybrid materials, using different *in-situ* synthetic pathways – hydrothermal and sol-gel;
ii. Evaluate the successful obtention of the hybrid materials through UV-Vis spectroscopy;
iii. Perform the structural elucidation of all hybrid materials by ATR-FT-IR; PXRD and Electronic Microscopy – SEM and TEM;
iv. Evaluation of the hybrid materials (at least two different morphologies resultant for the most promising synthetic approaches) for wound healing applications – materials cytotoxicity evaluated *via* PrestoBlue assay; and potential as wound healing materials assessed through *in vitro* scratch assay.

The innovative character of the work developed within this MSc project is based on studying the direct impact of different reaction parameters in *in-situ* approaches (hydrothermal and sol-gel methods) in the structure of the obtained hybrid materials.

2. Materials and Methods

2.1. Reagents

The reagents used in the synthesis methods are of analytical grade and used without further purification processes. Zinc chloride (> 98%), zinc acetate dihydrate (> 98%) and commercial ZnO nanopowder presenting with particles of less than 100 nm in size were purchased from Sigma-Aldrich (St. Louis, MO, USA). Ethanol (> 99.8%) was purchased from Honeywell (Buchs, Switzerland) and sodium hydroxide (> 99%) was purchased from LABCHEM (Zelienople, PA, USA). Cellulose nanocrystals (100 wt%) - white, odorless solid of cellulose sulfate sodium salt dried by using the spray-drying process – were purchased from CelluForce Inc (Canada).

2.2. Preparation of CNC/ZnO hybrid materials

Hybrid materials CNC/ZnO were prepared by using *in-situ* approaches based on hydrothermal and sol-gel methods. A detailed description of the reaction conditions studied in each method is provided in the following subsections.

2.2.1. Hydrothermal method

Two different strategies were employed with the use of two different zinc oxide precursors to determine its influence on morphology and/or other structural properties. This approach was used taking into consideration the evidences found in literature showing that different zinc oxide precursors originate particles with various morphologies i.e., zinc chloride produced flower-like ZnO structures on CNC surface[58], while zinc acetate dihydrate morphologies such as ZnO nanorods[82] and nanospheres[83].

In this manner, syntheses of materials using zinc chloride (**HS1**-**HS5**) and zinc acetate dihydrate (**HS6**-**HS8**) as distinct zinc oxide precursors were carried out.

The synthesis of material **HS1** was based on the reactional conditions described by Abdalkarim *et al.* (2018)[58]. Briefly, 10.0837 g of CNC were dissolved in 25 mL of deionized water, followed by the addition of 0.6821 g of $ZnCl_2$ and 0.6135 g of NaOH.

The solution was then heated in an oven at 80 °C for 24 h. The conditions to attain the materials (**HS2**-**HS5**) resulted from alterations of this protocol: in all cases, after the reaction, the materials were thoroughly washed with water (100 mL), followed by ethanol (25 mL), and dried overnight at 55 °C. The hybrid materials **HS2**-**HS5** were obtained in the following way:

HS2: The preparation of material **HS2** followed similar reactional conditions previously described for **HS1**, but was studied the ratio 1:0.2:0.2 for CNC/$ZnCl_2$/NaOH.

HS3: In the preparation of this hybrid material was investigated the following ratio 1:0.2:0.3 of CNC/$ZnCl_2$/NaOH, keeping the reaction temperature at 80 °C for 24 h.

HS4: This material was obtained by using the ratio 1:0.2:0.3 of CNC/$ZnCl_2$/NaOH, the same studied for **HS3**, but the reaction occurred at 100 °C for 66.5 h.

HS5: The hybrid material **HS5** in a similar way previously described for **HS4**, but using the ratio 1:0.6:0.5 for CNC/$ZnCl_2$/NaOH.

In the preparation of the materials **HS6-HS8** was studied a different zinc oxide precursor, the zinc acetate dihydrate. These materials were prepared in the following way:

HS6: For the obtention of the material **HS6** was used the following ratio 1:0.6:0.5 of CNC/$Zn(CH_3COOH)_2.2H_2O$/NaOH. The solution was heated at 100 ºC for 68 h, washed with water (100 mL), followed by ethanol (25 mL), and then dried overnight in an oven at 55 °C.

HS7: The material **HS7** was obtained by using the conditions previously described for **HS6**, but using a ratio of 1:0.2:0.3 for CNC/$Zn(CH_3COOH)_2.2H_2O$/NaOH.

HS8: The hybrid material was also obtained by using the reaction conditions described for **HS6**, but was studied the ratio 1:1.5:1.5 for CNC/$Zn(CH_3COOH)_2.2H_2O$/NaOH.

2.2.2. Sol-gel method

Three different hybrid materials were prepared by using the sol-gel method (**SG1**-**SG3**). The steps to afford these materials followed the study reported by Azizi *et al.* (2013)[74], but were studied different ratios of reagents, and also a different zinc salt - zinc acetate dihydrate.

All prepared materials followed the same steps: to a solution containing CNC and deionized water (12.5 mL), ethanol (15.5 mL) and zinc acetate dihydrate were added. The

obtained solutions were homogenized through magnetic stirring for 1 h at room temperature, followed by gentle stirring for 2 h at 80 °C. Then, NaOH (5 mol/L) was added dropwise. The materials were washed with deionized water (100 mL), and then placed in oven at 120 °C for 1 h, to allow conversion of remaining unreacted zinc hydroxide into zinc oxide. Synthesized products were left to dry in an oven at 55 °C for 6 h. The hybrid materials were then attained by using the following ratio for the reagents CNC/$Zn(CH_3COOH)_2.2H_2O$: 1:0.5; 1:1, and 1:1.5 for **SG1**, **SG2**, and **SG3**, respectively.

2.3. Characterization of CNC/ZnO Hybrid Materials

2.3.1. UV-Vis Spectroscopy

The UV-Vis spectra for the hybrid materials obtained by hydrothermal (**HS3**-**HS8**) and sol-gel methods (**SG1**-**SG3**) were performed according to the procedure previously described by Yu *et al.* (2015)[85] with some modifications. Briefly, aqueous solutions at 0.06% (w/v) were analyzed on a BioTek Epoch 2 microplate reader in the spectral range of 300 to 700 nm. All analyses were performed in triplicate.

2.3.2. Attenuated Total Reflection Fourier-Transform Infrared (ATR-FT-IR) Spectroscopy

The ATR-FT-IR spectra of the CNC/ZnO hybrid materials (**HS3**-**HS8** and **SG1**-**SG3**) and the CNC building unit were recorded using Frontier™ MIR/FIR spectrometer from PerkinElmer with a reading spectral range between 550 to 4000 cm^{-1} for 8 scans and a spectral resolution of 4 cm^{-1}. All analyses were performed at least in duplicate.

2.3.3. Powder X-ray Diffraction (PXRD) analysis

The Powder X-ray diffraction (PXRD) analyses for the hybrid materials (**HS3**-**HS8** and **SG1**-**SG3**), as well as for CNC and ZnO were performed on a Rigaku MiniFlex 600 diffractometer utilizing a Cu kα radiation at a voltage of 40 kV and a current of 15

mA ($3^o \leq 2\theta \geq 100^o$; step of 0.01 and speed rate of 3.0°/min). All analyses were conducted at least in duplicate.

2.3.4. Electronic Microscopy analysis

Scanning Electron Microscopy (SEM)

The SEM analyses for the hybrid materials (**HS3**-**HS8** and **SG1**-**SG3**), and for CNC and ZnO were performed using a Thermo Scientific™ Pro Scanning Electron Microscope to observe the hybrids' morphology. Before the analysis, the samples were prepared by being placed in observation stubs using double-sided adhesive carbon tape as fixation material (NEM tape) and then coated with Au/Pd (target SC510-314B from ANAME, S.L., Madrid, Spain) *via* Sputter Coater (Polaron, Bad Schwalbach, Germany). Samples' analyses were performed under high vacuum medium and with an acceleration voltage of 10 kV.

Transmission Electron Microscopy (TEM)

The morphology of the hybrid materials **HS6** and **HS8** obtained by the hydrothermal synthesis, as well as the morphology of CNC and ZnO were also investigated by TEM. All analyses were performed using a JEOL JEM 1400 TEM equipment (Tokyo, Japan) at 120 kV voltage. Digital images were extracted from a CCD digital camera (Orious 1100W, Tokyo, Japan) at the HEMS/i3S institute of the University of Porto.

For samples' preparation, 10 µL of each sample was loaded onto Formvar/carbon film-coated mesh nickel grids (Electron Microscopy Sciences, Hatfield, PA, USA) and left standing for 2 minutes. Excess liquid was then removed using filter paper, and each different grid maintained contact with a drop of uranyl acetate at 2% (*w*/*v*) for 2 minutes at a time.

2.4. Cytotoxicity evaluation

The cytotoxicity evaluation was performed by PrestoBlue assay, according to ISO 10993-5: 2009 (E) and considering the recommendations of ISO 10993-5:2. The PrestoBlue assay was performed according to the manufacturer's instructions using the human keratinocyte cell line HaCaT (CLS, Germany). Cells were kept in culture in DMEM media (Gibco) supplemented with 10% FBS (Gibco) and 1% antibiotic (Gibco) at 37 ºC, with 5% CO_2 in a humidified atmosphere. For the assays, these cells were seeded, at a concentration of $1x10^4$ cells/well, in 96-well plates and incubated to allow cellular adhesion.

Hybrid materials selected for cytotoxicity tests, previously sterilized with UV radiation, were prepared with a concentration of 1 mg/mL of media (w/v). From that concentration, 5 successive dilutions were prepared for each sample with a 1:2 ratio. The solutions were added to the cells and incubated for 24 h. PrestoBlue reagent was added to the 96-well plates and incubated for 3 hours. The fluorescence signal was read in a BioTek Synergy H1 microplate reader (USA). The results are expressed in percentage of cell viability as compared with a control (cells without treatment). At least two independent experiments were performed.

2.5. Wound healing assessment by *in vitro* scratch assay

The wound healing assessment was performed *via* scratch assay using HaCaT cells seeded into sterilized ibidi® µ-Plate 24 Well Black ID 14 mm ibiTreat. The plate had a gap, similar to a scratch made by a pipette tip or needle, between monolayer of cells that mimics a wound. Cells were seeded at 50000 cells per insert and were left to adhere for 24 h. Then, cells were treated with Mitomycin C at 25 µg/mL for 2 h to block cell proliferation before the addition of the hybrid composites. Dispersions of hybrid materials selected for wound healing assay were prepared in media with concentrations of 200 µg/mL and 50 µg/mL according to the cytotoxicity observed for each compound. For ZnO a concentration of 20 µg/mL was used.

Photographs were taken using a Primovert inverted microscope (Zeiss) and Zen software (Zeiss) at 0 h, 18 h, 24 h and 42 h of cells exposure to added hybrid composites. At each timepoint the cells were washed with PBS solution to remove influence of the

hybrid materials in the image capture. The wound area for wound healing evaluation was quantified using ImageJ software.

3. Results and Discussion

In-situ approaches were employed for the obtention of hybrid materials CNC/ZnO based on the hydrothermal and sol-gel synthesis methodologies. The detailed reaction conditions studied in the two methodologies are described in the subsections below.

In order to confirm successful obtaining of the CNC/ZnO hybrids, UV-Vis spectroscopy was performed. Posteriorly, structural features of these hybrid materials were characterized by: ATR-FT-IR, for evaluation of the vibrations of the functional groups characteristic of cellulose; PXRD, to observe their diffraction pattern and crystallinity and by electronic microscopy (SEM and TEM) for observation of their morphology. Hybrids with the most potential in terms of synthesis methodology and/or distintictive structural characteristics were selected for study of wound healing potential through the study of cytotoxicity with PrestoBlue assay, and wound healing evaluation *via in vitro* scratch assay.

3.1. Preparation of the CNC/ZnO hybrid materials

In the first instance, obtaining CNC/ZnO hybrids was explored through hydrothermal and sol-gel syntheses from Abdalkarim *et al.* (2018)[58] and Azizi *et al.* (2013)[74], respectively. Concerning issues found with the employed methodology and, with the intention to explore the impact of change in reaction conditions in the obtaining of different methodologies, different reaction parameters, including different ratios (e.g., ratio of CNC to zinc salt), different temperatures, reaction time and washing cycles were explored.

Pertaining to the hydrothermal synthesis method, there are reportedly many advantages, such as the obtaining of final products with high purity and crystallinity, with no requirement for organic solvents that may negatively affect the environment with the release of toxic by-products during the synthesis reactions. This, combined with the bypassing of the need for additional processing, in theory, is the main motivation for the choice on one of the synthetic methods employed in this work. [44,45,58,61,63]

On the other hand, sol-gel synthetic approach has similar advantages to hydrothermal ones in terms of ease of execution, minimal reagents requirement as well as repeatability. However, hybrid materials synthesized by this method reportedly took

less time in terms of reaction time during preparation of materials, as well as drying time, making for a more sustainable synthetic method. [62,74] As such, this encompasses the main motivation for the choice of this approach in this work.

3.1.1. Hydrothermal process

For the *in-situ* synthesis of CNC/ZnO hybrids *via* the hydrothermal method, the reaction conditions reported in Abdalkarim *et al.* (2018)[58] where firstly evaluated.

Below, Table 3 encompasses all materials prepared by the hydrothermal method and the detailed reaction conditions applied, where a change in reactional parameters was introduced with the exploration of different reagents ratio, different reaction temperature and time, and different zinc salts in order to ascertain their impact in the materials' structural features.

Table 3. Reaction conditions applied in the hydrothermal synthesis to attain CNC/ZnO hybrid materials (**HS3**-**HS8**).

Reaction Conditions	CNC/ZnO Hybrid Materials							
	HS1	**HS2**	**HS3**	**HS4**	**HS5**	**HS6**	**HS7**	**HS8**
Solvent	Deionized water (25 mL)							
Zinc Chloride (g)	0.6821	2.0025	0.6845	0.6840	0.6788	_____	_____	_____
Zinc Acetate Dihydrate (g)	_____	_____	_____	_____	_____	0.6917	0.6945	1.8211
Sodium hydroxide (g)	0.6135	1.8133	0.6005	0.6001	0.6019	0.5981	0.5968	1.7930
Cellulose nanocrystals (g)	10.0837	10.0420	2.5108	2.5353	1.2105	1.1894	2.4934	1.2085
Temperature (°C)	80			100				
Reaction Time (h)	24			66.5		68		
Washing solvents	_____	_____	Deionized water; ethanol					
Washing cycles	_____	_____	6	9		8		
Drying temperature (°C), overnight	_____	_____	55					
Mass of the hybrid material (g)	_____	_____	1.1813	1.9788	0.5511	0.7085	1.6108	0.9135

In total, eight different materials were prepared *via* hydrothermal synthesis and will be referred to, in order of synthesis, as materials **HS1**-**HS8**. Two different approaches were tested, by using different zinc salts: zinc chloride for materials **HS1**-**HS5** and zinc acetate dihydrate for **HS6**-**HS8**.

Reaction conditions described in Abdalkarim *et al.* (2018) [58] served as base for obatining of material **HS1** and **HS2**, where the latter had a change of reagents ratio introduced.

Seeing that the final mixture of the first two initial preparations displayed a pasty texture, which was hard to resuspend in distilled water for washing step, those materials (**HS1** and **HS2**) were excluded from core analysis characterization.

For material **HS3**, reaction conditions used for **HS1** were replicated changing the quantity of CNC, which was lowered to 2.5 g to try and achieve a better dispersion with mixture of zinc chloride, sodium hydroxide and distilled water, before placement in oven. Having observed a product with solid and liquid phase, is can be deduced that final mixture had a better dispersion.

A change in reagents ratio based on the reaction conditions of material **HS3** was explored for the other hydrothermal synthesis materials (**HS4**-**HS8**), as well as an increase of reaction time to 66.5 h for materials **HS4** and **HS5** and 68 h for **HS6**-**HS8**, and an increase of the reaction temperature (80 to 100 ºC) for **HS4**-**HS8** .

Materials that were washed *via* centrifugation (**HS3-HS8**), represented in Figure 15, were dried in oven at 55 °C and took 6 hours to fully dry. The drying temperature in this case is slightly lower than the one employed in Abdalkarim *et al.* (2018) [58], which was 60 °C and, seeing that it took practically half the time for drying, compared to the reported 12 h, we can observe optimization in our hydrothermal synthetic approach when it comes to drying time of the obtained materials, since less time means less resources consumption and a more economical synthetic approach.

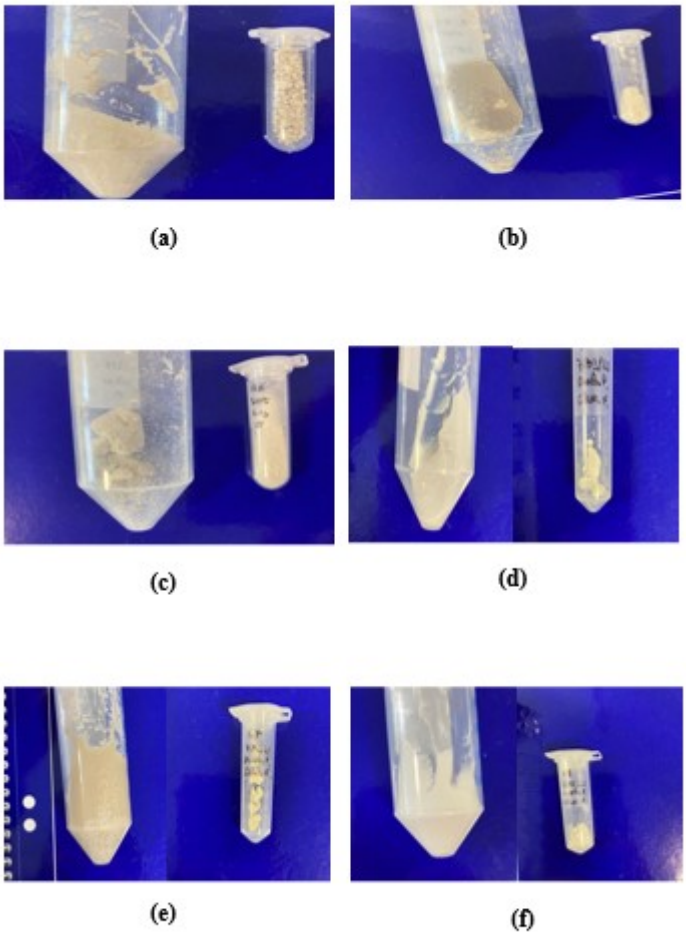

Figure 15. Synthesized hydrothermal hybrid materials with (**a**), (**b**), (**c**), (**d**), (**e**) and (**f**) representing materials **HS3**, **HS4**, **HS5**, **HS6**, **HS7** and **HS8**, respectively. In each image there is a sample of the material before (left) and after (right) drying in oven.

Before drying of whole material, samples were extracted for material characterization and to observe the behavior of obtained materials under environment at 55 °C for an extended period of time (in this case, overnight).

The successful obtaining of the hybrids was assessed *via* UV-Vis spectroscopy, as seen in Figure 16.

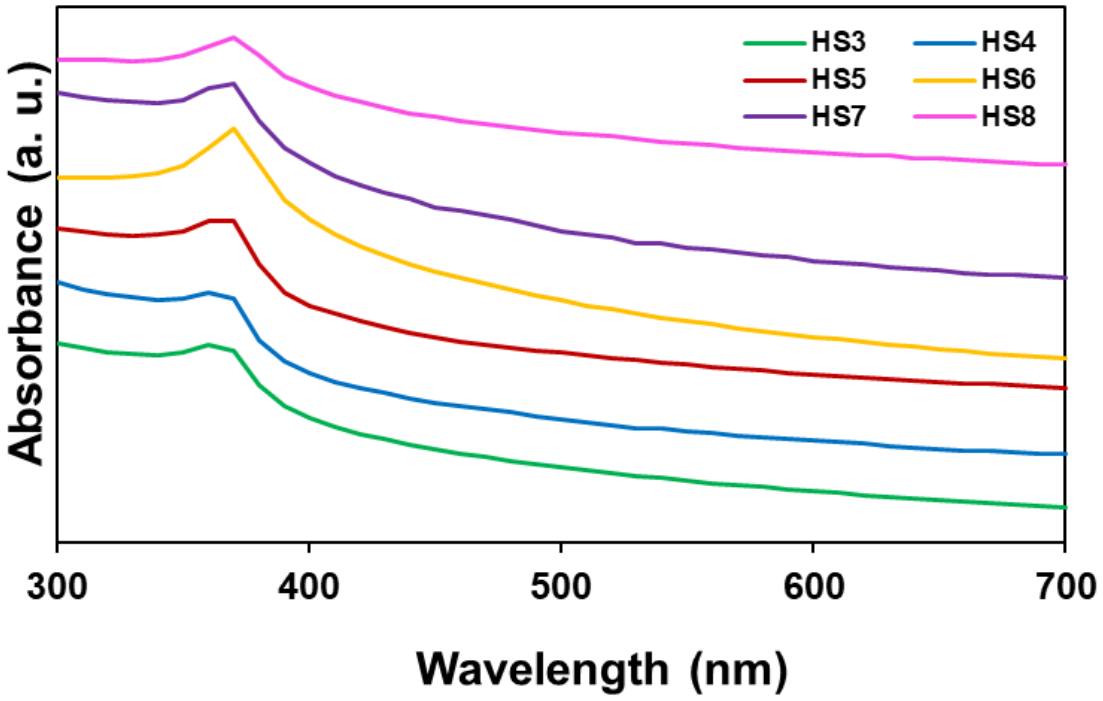

Figure 16. UV-Vis spectra of the CNC/ZnO hybrids obtained by hydrothermal synthesis (**HS3-HS8**).

This characterization technique allows the confirmation of successful hybrid formation since in the region of 300 to 700 nm there is a characteristic absorbance peak from 356 to 367 nm, according to Yu *et al.* (2015)[85] that is attributed to the presence of ZnO and CNC alone did not present with any relevant peak in the spectrum of 300 to 700 nm.

The peaks observed with maximum absorbance at 360 and 370 nm (Figure 16) indicate successful formation of zinc oxide on CNC surface, which correspond to the expected results from previous literature.[85]

Materials **HS3** and **HS4** of hydrothermal synthesis showed maximum absorbance at lower wavelength, 300 nm (Figure 16).

This event is attributed to a blue shift, which describes a change in absorbance to a shorter wavelength, and may suggest changes in either morphology, shape, or size of formed zinc oxide nanoparticles, according to Azizi *et al.* (2013).[74]

On the other hand, Yu *et al.* (2015), reported a red shift, which is the opposite of a blue shift, describing a change of absorbance to a longer wavelength, and relate it to an increase in size of ZnO particles which could be directly related to Zn^{2+} ion concentration.[85]

In the results obtained herein, this change in absorbance may be due to the decrease in size of ZnO particles. In Wahyuono *et al.* (2016), a direct correlation between the increase in ZnO crystallite size and the increase of annealing temperature is observed from synthesized ZnO particles.[77]

3.1.2. Sol-gel process

Pertaining to the *in-situ* sol-gel approach for obtaining CNC/ZnO hybrids, the reaction steps reported by Azizi *et al.* (2013)[74] were taken into consideration. The authors synthesized hybrids of CNC/ZnO *via in-situ* sol-gel method with different ratios of zinc salt to CNC. Hybrid with the most promising characteristics from structural and thermal characterization was chosen for antimicrobial evaluation, which was compared against ZnO nanoparticles alone, and the authors found that the hybrid performed better.[74]

Considering that there are reports of different ZnO morphologies using the same zinc salt, namely zinc acetate, a change in ratio of zinc oxide precursor to CNC was introduced in this work to explore the effects on the material structure.[62,74] Below, Table 4 summarizes all reaction conditions for the different materials prepared by sol-gel method.

Table 4. Reaction conditions applied in the sol-gel synthesis to attain CNC/ZnO hybrid materials (**SG1**-**SG3**).

CNC/ZnO hybrid material	**SG1**	**SG2**	**SG3**
Solvent	Deionized water (12.5 mL)		
Cellulose nanocrystals (g)	1.1983	1.2108	1.1975
Zinc Acetate Dihydrate (g)	0.6116	1.2196	1.8025
Ethanol (mL)	15.5		
Sodium hydroxide (M)	5		
Mixing time (h)	1		
Reaction time (h)	2 + 1		
Reaction temperature (°C)	80, followed by 120		
Washing solvent	Deionized water		
Washing cycles	5		
Drying temperature (°C), overnight	55 °C		
Mass of the hybrid material (g)	0.2921	0.2354	0.4118

The steps to attain the materials **SG1**-**SG3** followed the methodoly previously described were by Azizi et al. (2013)[74], but a different zinc salt was used (zinc acetate dihydrate), being also explored different reagent ratios of CNC/Zn($CH_3COOH)_2.2H_2O$:1:0.5; 1:1, and 1:1.5 for **SG1**, **SG2**, and **SG3**, respectively.

From hydrothermal approach to sol-gel one the number of wash steps was moderately lower.

Authors Azizi *et al.* (2013) [74] were able to obtain dry materials after the preparation step with placement in oven at 120 °C for 1 h. However, in this case, prepared materials needed further drying. As such, drying conditions applied for materials prepared with hydrothermal approach were employed.

In the materials obtained by the sol-gel methodology (Figure 17) was observed the occurrence of volume shrinkage and cracking of material during drying, which is a known possible disadvantage from this synthetic approach reported in Carter *et al.* (2007).[46]

(a) (b) (c)

Figure 17. Synthesized sol-gel hybrid materials with (**a**), (**b**) and (**c**) representing materials **SG1**, **SG2** and **SG3**, respectively where in each image there is a sample of the material before (left) and after (right) drying in oven.

In a similar way to the materials of hydrothermal synthesis, formation of CNC/ZnO hybrids was confirmed through UV-Vis spectroscopy and this evaluation can be observed in Figure 18 below.

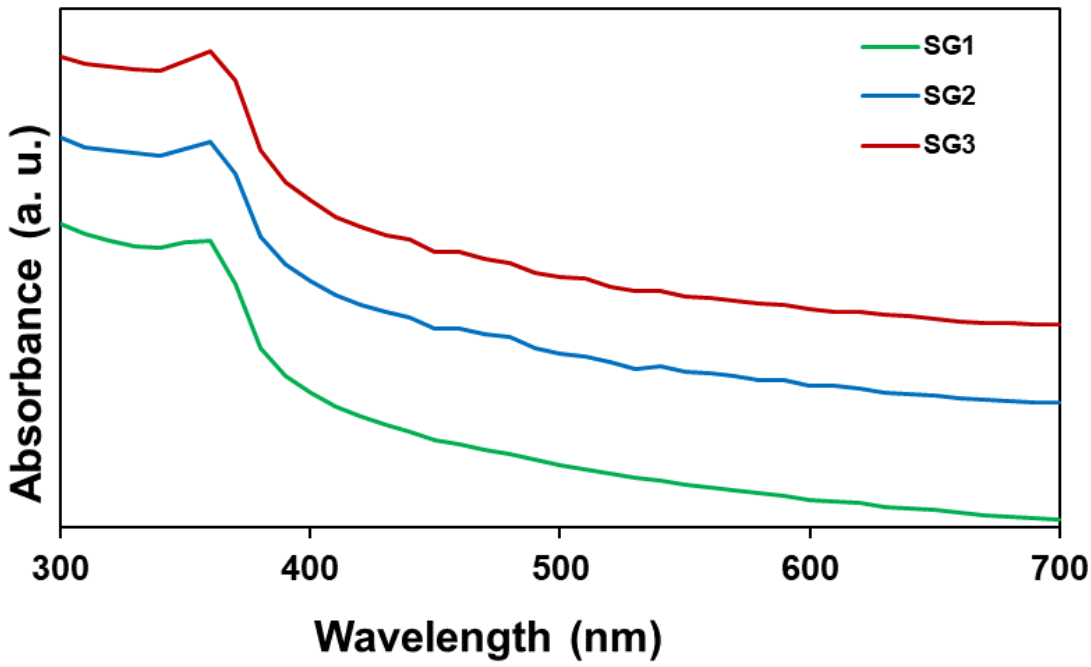

Figure 18. UV-Vis spectra of the CNC/ZnO hybrids obtained by sol-gel synthesis (**SG1-SG3**).

As with hydrothermal synthesis, hybrid characteristic peak at 360 nm was also observed with material **SG3** (Figure 18). However, a blue shift was observed with materials **SG1** and **SG2**, which may be associated with changes in either shape, size or morphology of ZnO particles according to related literature.[74]

Since the quantity of CNC was fairly similar for all sol-gel preparations, there is a possible influence of the zinc oxide precursor as for the first two preparations (**SG1** and **SG2**) the quantity of zinc acetate dihydrate is lower than the third sol-gel preparation final product (**SG3**). As such, it is reasonable to relate the change in maximum absorbance to the change in zinc oxide precursor quantity and, therefore, Zn^{2+} ion concentration, as reported in Yu *et al.* (2015).[85]

3.2. Structural Features of the CNC/ZnO Hybrid Materials

Hybrids composed of CNC/ZnO obtained through hydrothermal (**HS3**-**HS8**) and sol-gel (**SG1**-**SG3**) syntheses were evaluated on a structural level *via*: ATR-FT-IR spectroscopy, that allowed the conservation of samples since the covalent bonds remain intact and, similarly to UV-Vis spectroscopy, allowed the visualization of the stretching and bending vibrations characteristic to certain functional groups of the composites, namely nanocellulose[66,68,70]; PXRD analysis, useful for determination of unknown compounds and is based on the evaluation of the diffraction pattern of a crystalline structure, that is, the structural arrangement of atoms present in the samples[61,68,71] and *via* SEM and TEM microscopy which allowed the observation of the disposition of particles and cellulose nanofibers, providing information relative to morphology and their dimension, as well.[66–71]

3.2.1. ATR-FT-IR spectroscopy

Figure 19 below contains all ATR-FT-IR spectra of CNC/ZnO hybrids obtained by *in-situ* hydrothermal (**HS3**-**HS8**) and sol-gel (**SG1**-**SG3**) approaches as well as of CNC used in the synthesis of the hybrids.

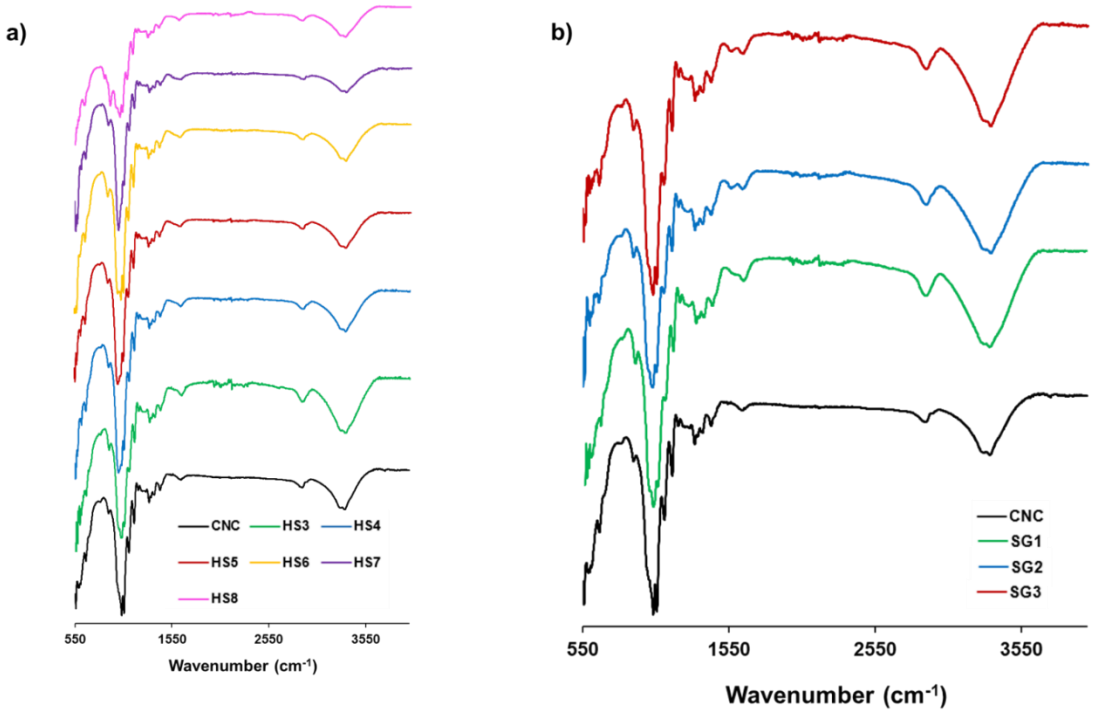

Figure 19. ATR-FT-IR spectra of CNC, **a**) materials from hydrothermal (**HS3**-**HS8**) and **b**) sol-gel (**SG1**-**SG3**) syntheses.

In this work, ATR-FT-IR spectra have a limited reading spectra from 550 to 4000 cm^{-1} wavenumber. As such, the region of 430 to 442 cm^{-1} described in Azizi *et al.* (2013) cannot be observed, which represents the stretch bands of zinc and oxygen.[74]

However characteristic peaks of prepared hybrids at 3337 and 1377 cm^{-1} attributed to the stretching and bending of hydroxyl groups can be distinguished in the hybrids from hydrothermal (**HS3**-**HS8**) and sol-gel (**SG1**-**SG3**) preparation.

According to the work of Aguayo *et al.* (2018), it is possible to observe a peak at 900 cm^{-1} (C-H rocking) which is attributed to the glycosidic linkages (Figure 19).[86,87] The presence of stretching vibration bands at 1060, 1110 and 1161 cm^{-1} associated to the C-O-C ring are characteristic of cellulose functional groups and, in turn, of CNC. In the range of 1420 to 1430 cm^{-1} the peaks that can be observed are attributed to the symmetric bending of CH_2, which can also be found in cellulose molecular structure. Furthermore, between 1330 to 1380 cm^{-1} bending vibrations attributed to the C-H and C-O groups of cellulose polymers (polysaccharides) are also observed.[87]

From the literature, the vibration band observed in the range of 1642-1650 cm^{-1} is associated with adsorbed water in cellulose (O-H bending)[86], as described by Aguayo *et al.* (2018) and Yu *et al.* (2015).[85,87] Other characteristic peaks from cellulose can also be

noted, such as the ones attributed to the hydroxyl group at 3337 cm^{-1} and 1377 cm^{-1}, representing stretching and bending vibrations. Furthermore, a characteristic peak attributed to the pyranose ring ether band at 1050 cm^{-1} is also present. The peak in the region of 2800 to 2900 cm^{-1} is attributed to the stretching band of the C-H. [85–87]

The main spectra that differ from the literature are the ones from **HS3** and **HS8** (Figure 19), with varying intensities around the 1050 cm^{-1} region, attributed to the C-O-C ring characteristic of cellulose.

The FT-IR spectra of sol-gel materials (**SG1**-**SG3**) appear to show the same characteristics peaks attributed to nanocellulose that were mentioned earlier for materials of hydrothermal synthesis (Figure 19), corroborating current literature on the subject.[85,87]

3.2.2. PXRD analysis

The PXRD patterns of the CNC/ZnO hybrids obtained by *in-situ* hydrothermal (**HS3**-**HS8**) and sol-gel (**SG1**-**SG3**) approaches, as well as PXRD patterns of the CNC building unit and of commercial ZnO sample can be observed in Figure 20.

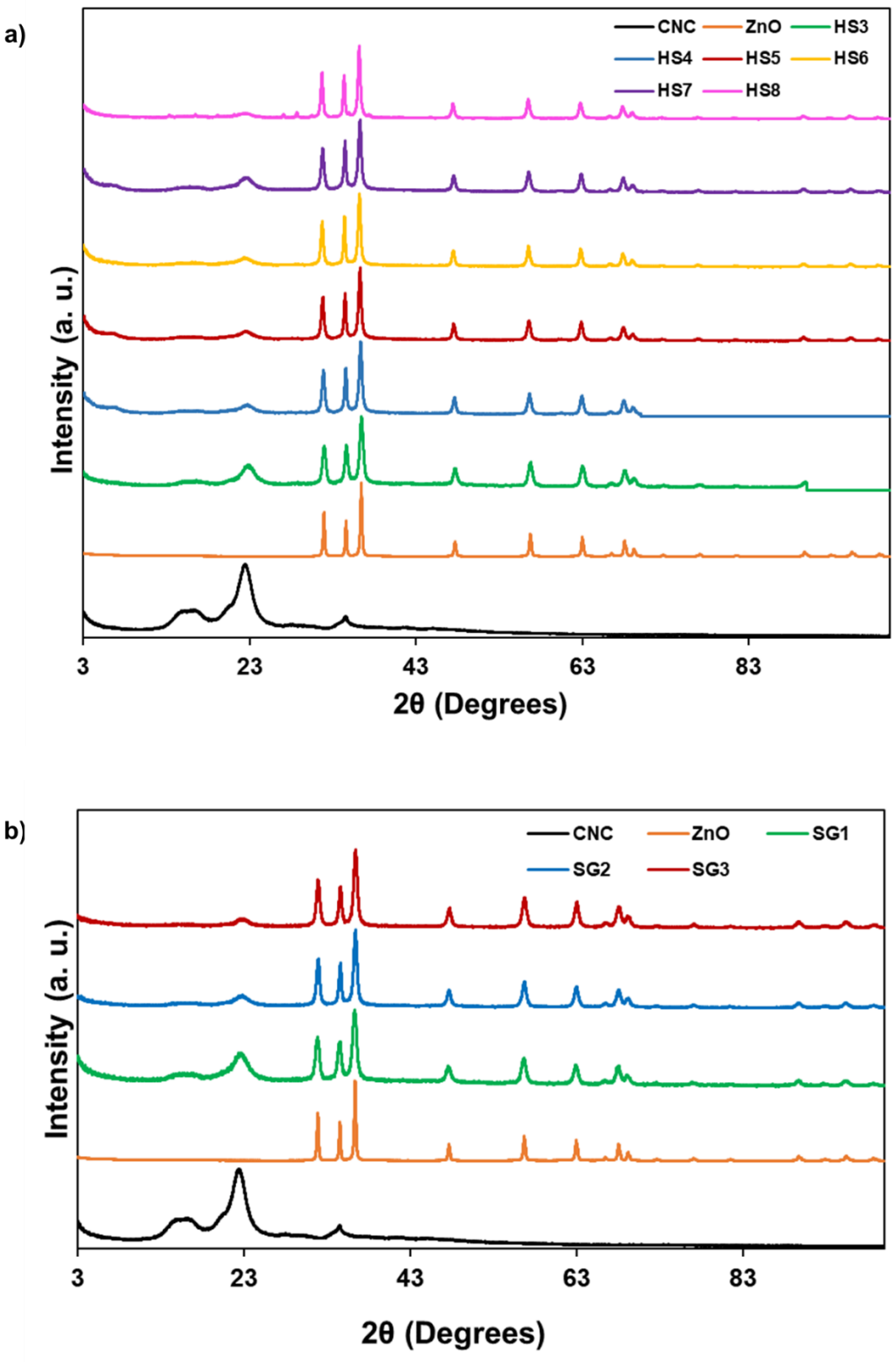

Figure 20. PXRD patterns of CNC and commercial ZnO as well as of materials from **a**) hydrothermal (**HS3**-**HS8**) and **b**) sol-gel (**SG1**-**SG3**) syntheses.

All the materials attained through hydrothermal (**HS3**-**HS8**) and sol-gel (**SG1**-**SG3**) syntheses exhibited the characteristic reflections of ZnO at 2θ = 31.7°, 34.4°, 36.2°, 47.5°, 56.4°, 62.9°, 67.7° and 69.1°.Additionally, it is also possible to observe, in all PXRD patterns, the characteristic reflections of CNC (cellulose I) at 15.1°, 16.4°, 22.7°, and 33.9°.[74,85] These findings also corroborate the successful obtention of the CNC/ZnO hybrid materials in all cases.

In the materials obtained by the hydrothermal process, it is possible to observe a lower peaks intensity in materials **HS3** and **HS4** (Figure 20), suggesting a smaller crystal size and crystallinity, in both cases, which contrasts with the results obtained to the material **HS8** – highest reflection intensities suggesting an increased size of ZnO. .[85]

Regarding the materials obtained by the sol-gel method, the PXRD pattern of **SG3** showed increased peak intensities than the other materials, suggesting that a higher concentration of the zinc salt resulted in a material with a higher crystal size.

3.2.3. Electronic Microscopy

With SEM and TEM microscopy we can observe the structure of the hybrids, allowing us to identify morphology of ZnO particles dispersed in cellulose nanocrystals matrix and particles dimension. The choice to employ both types of electronic microscopy stems from the different type of information that they provide: SEM microscopy as a scanning image with information about the sample surface and TEM microscopy as a transmission image providing information about the inner structure of the sample with near-atomic resolution.[66–71,88]

3.2.3.1. SEM microscopy

Below, Figure 21 contains SEM images of materials prepared by hydrothermal method (**HS3**-**HS8**). SEM images of CNC (building unit) and of ZnO commercial sample were included for a better comparison between those and obtained hybrid composites.

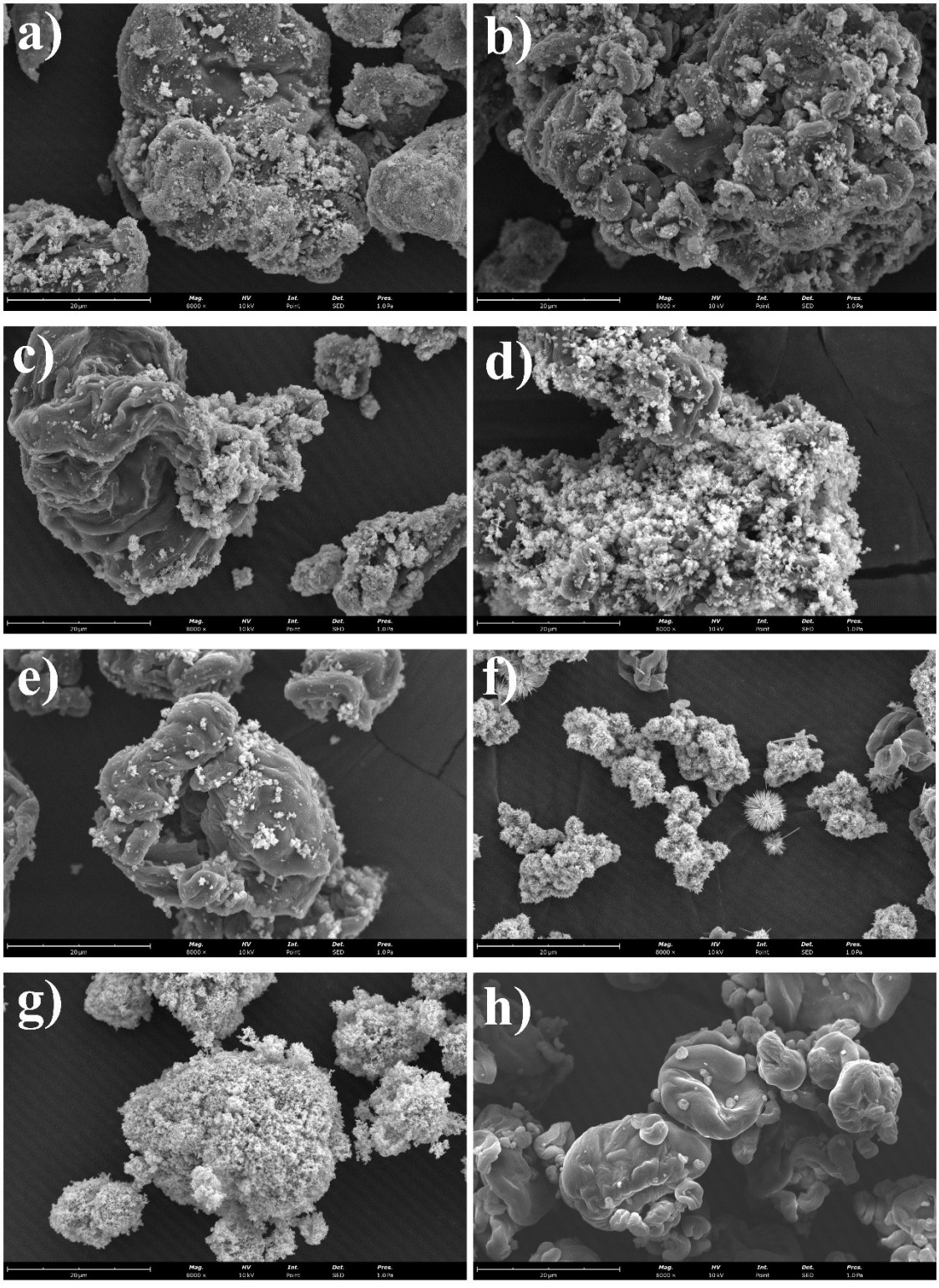

Figure 21. SEM images (8000 x ampliation) of hydrothermal materials: **a**) **HS3**, **b**) **HS4**, **c**) **HS5**, **d**) **HS6**, **e**) **HS7** and **f**) **HS8**, as well as of construction units of the hybrids where **g**) ZnO particles and **h**) CNC.

All materials except material **HS8** exhibited a similar ZnO morphology that can be identified as being irregular agglomerates (Figure 21), considering the reports with similar morphology on hybrids with identical construction units.[68,76]

Material **HS8** (Figure 21) presented with at least two different morphologies: flower-like, according to observed morphology from previous literature[58,61,63,66,73], and sea urchin-like that could be considered a transitory state for flower-like morphology due to long and thin rod-like morphology in the sea urchin-like ZnO particles. This suggests lower crystallinity of the particles compared to flower-like, that requires longer crystallization time, despite the reduced size. The transitory state to flower-like morphology is also suggested due to findings reported by Wahyuono *et al.* (2016), with observation of intermediate structure: "screw-drive" to nanoflower.[77] Abdalkarim *et al.* (2018) observed transition from uniform nanosheet to flower-like on the surface of CNC from prepared hybrids, also sustaining the possibility that sea urchin-like morphology observed in this work may be a transitory state for flower-like morphology.[58]

Similarly to Figure 21, the figure below (Figure 22) comprises SEM images of prepared sol-gel materials (**SG1**-**SG3**), commercial ZnO nanopowder and CNC from CelluForce.

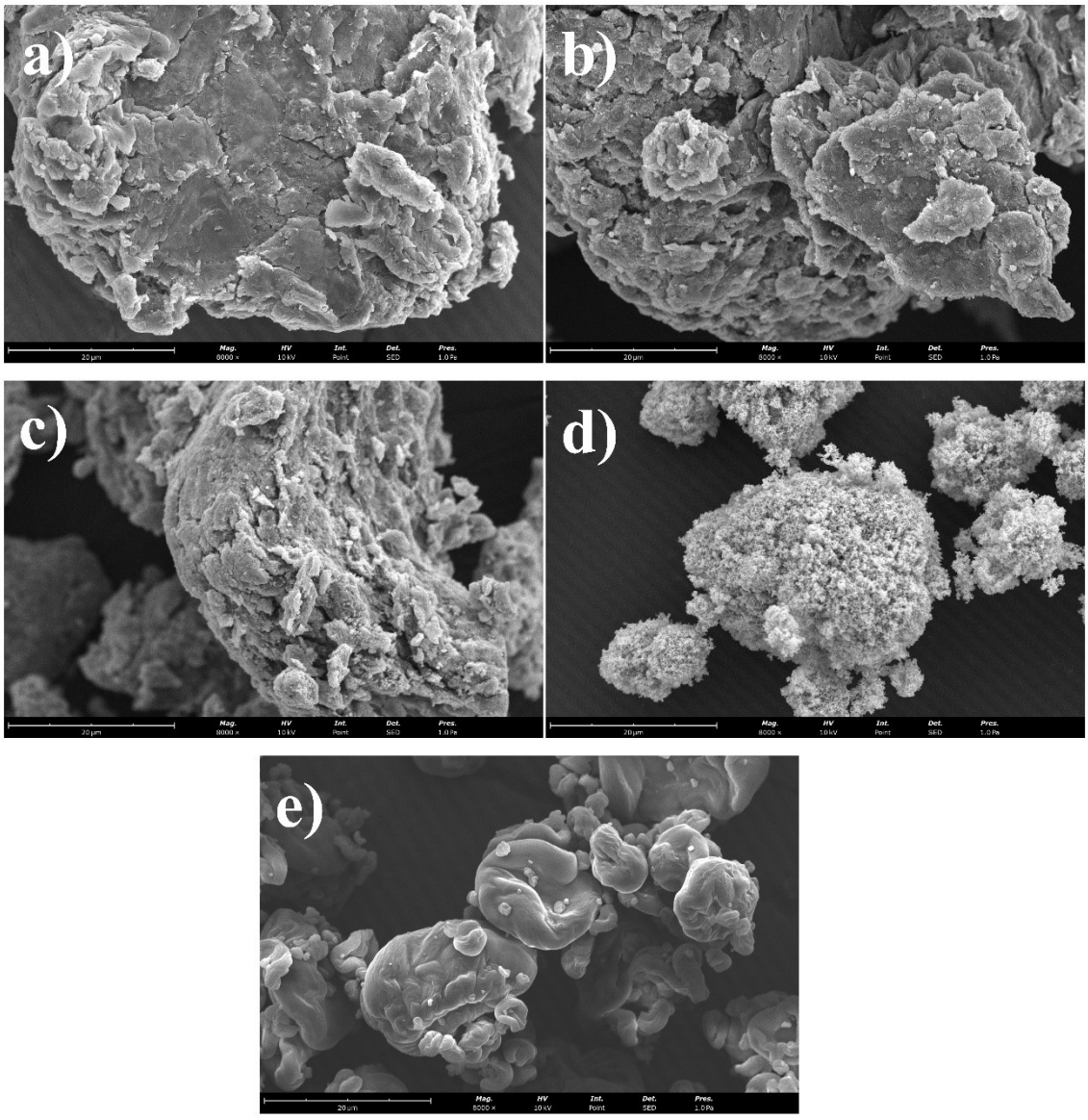

Figure 22. SEM images (8000 x ampliation) of sol-gel materials with **a**) **SG1**, **b**) **SG2**, **c**) **SG3** and of: **d**) commercial ZnO particles sample and **e**) CNC from CelluForce.

Morphology of ZnO particles of sol-gel synthesis materials (Figure 22) most likely can be defined as irregular agglomerate shapes, following the same rational as the one mentioned above for the hybrid composites prepared through hydrothermal synthesis.[68,76]

SEM images (Figure 21 and Figure 22) of the hybrids show amorphous agglomerates akin to a tightly "packed structure" that, according to Abdallah *et al.* (2018), suggest presence of CNC agglomerates.[89]

Observing the SEM profile of CNC and ZnO in separate, a clearer distinction between those can be made in the synthesized hybrids, where ZnO particles obtained from employed *in situ* synthetic approaches (Figure 21 and Figure 22) are visible as distinct agglomerates in the CNC surface. This fact, along with the suggestion made above, supports the success in the hybrids preparation, a finding that corroborates with the results from the previous analyses.

From a cursory view and considering that all SEM images have the same ampliation (8000 x) and scale (20 μm), hybrid composites derived from sol-gel preparation (Figure 22) formed bigger irregular agglomerates compared to hydrothermal synthesis ones (Figure 21).

3.2.3.2. TEM microscopy

TEM analysis will only include the hybrids **HS6** and **HS8**, which had the most promising potential for wound healing study based on the distinctive morphology observed *via* SEM and TEM microscopy, and based on the fact that hydrothermal synthesis is considered to be the greenest approach in this work from the comparison between the two synthesis methods herein employed. Therefore, the Figure 23 below contains TEM images of materials **HS6**, **HS8**, commercial ZnO nanopowder and CNC from CelluForce.

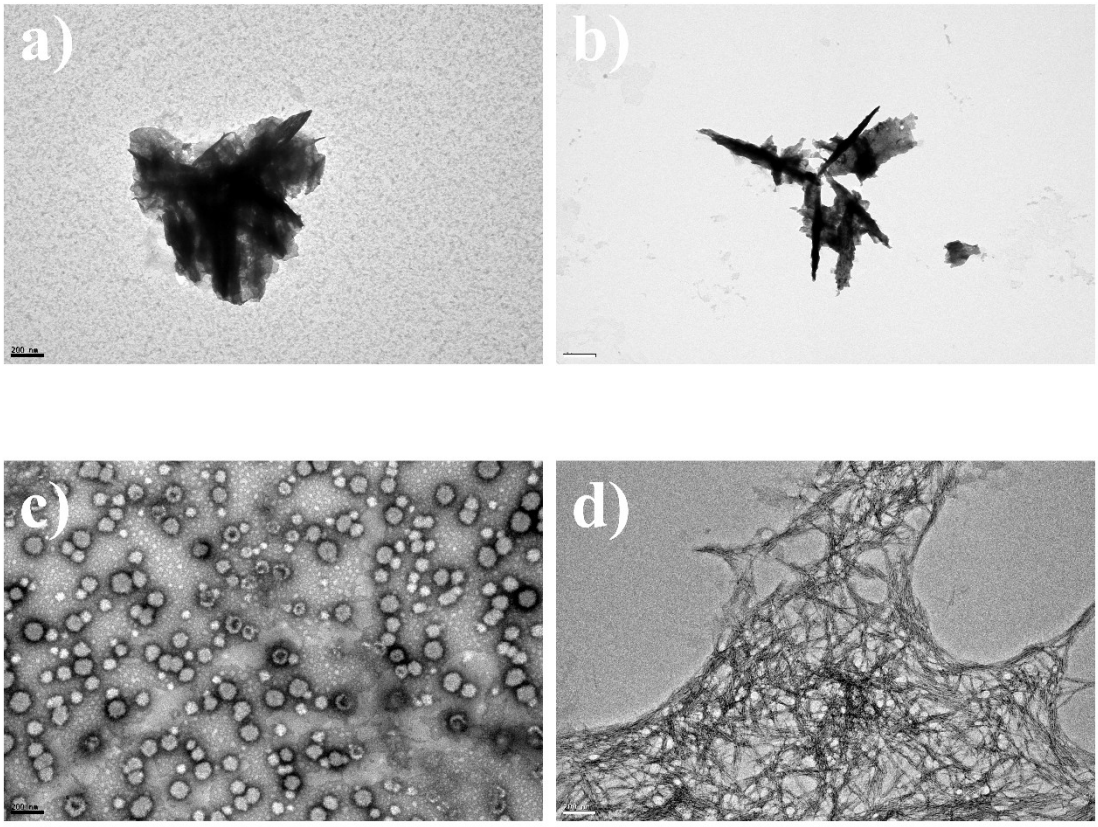

Figure 23. TEM images (50000 x ampliation) of hydrothermal materials: **a**) **HS6** and **b**) **HS8** as well as **c**) ZnO commercial sample and **d**) CNC from CelluForce.

Material **HS6** presents with nanorod-like morphology of ZnO according to the TEM image (Figure 23), a morphology that is reported in Hafez *et al.* (2014), Kumar *et al.* (2011), Janpetch *et al.* (2016), and Sahoo *et al.* (2020).[62,69,75,83] On the other hand, material **HS8** presents with flower-like morphology of ZnO which is more defined.

In both hybrids (**HS6** and **HS8**) a good dispersion of ZnO particles (dark agglomerates) on cellulose matrix is observed, and the latter (CNC) presents with a reticular shape (gray fibers), according to TEM images in Figure 23.[74,85]

3.3. Safety evaluation: selection of materials and their properties

3.3.1. Selection of materials for safety evaluation

For safety evaluation the aim was to select materials with, at least, two different morphologies. Having obtained materials with three different morphologies from hydrothermal synthesis approach, materials **HS6** and **HS8** were selected for cytotoxicity evaluation. These were selected due to their distinctive morphology including nanorods and sea urchin-like as well as due to hydrothermal synthesis method being a greener approach in terms of hybrids preparation, with less resources consumption, compared to sol-gel approach employed in this work. Hybrid materials' concentrations were chosen for wound healing assay depending on toxicity profile observed in cytotoxicity assay. These considerations also applied to the construction units of the prepared hybrids: CNC from CelluForce and ZnO nanopowder from Sigma-Aldrich, both commercial products used as control.

3.3.2. Cytotoxicity assay

Considering that this assay follows the protocol of ISO 10993-5:2, a sample is considered to exert significant cytotoxicity against studied HaCaT cell line when the material suppresses 30% or more of cells' metabolic activity.

Figure 24 shows the metabolic inhibition exerted by the hybrid materials and construction units' dispersions on HaCaT cells.

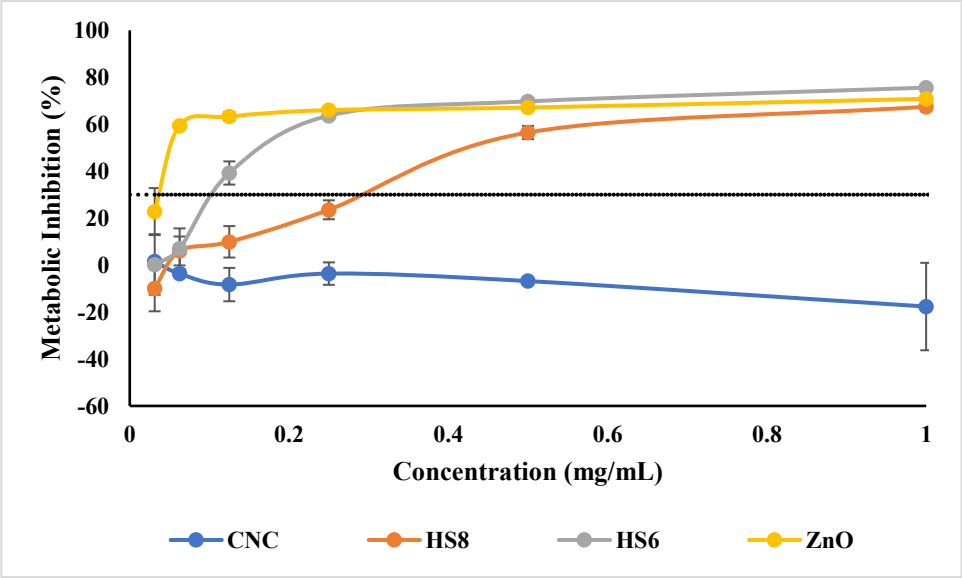

Figure 24. Impact of hybrid materials **HS6** and **HS8**, and of CNC and ZnO nanopowder commercial products used as control, at 20 µg/mL, 50 µg/mL and 200 µg/mL upon HaCaT cells metabolic activity. The dotted line represents the 30% cytotoxicity limit as defined by the ISO 10993-5:2.

As is possible to see from Figure 24, the CNC displayed non-toxic profile with negligible metabolic inhibition, as expected taking in consideration the data present in literature.[12,20,33] However, hybrid materials evaluated in this assay had significant toxicity for concentrations higher than 0.0625 mg/mL for **HS6** and at 0.25 mg/mL for **HS8**.

This may be due to a variety of factors such as presence of ZnO particles, synthesis conditions, or synthetic approach of the material among others.[12] Studies pertaining wound healing/dressing applications of hybrid materials comprising ZnO particles and other forms of nanocellulose, namely BNC and CNF, have reported significant biocompatibility with other cell lines, including human dermal fibroblasts and L929 fibroblast cells.[68,71,76]

In this work, ZnO particles alone displayed the most significant toxicity effect for concentrations higher than 0.031 mg/mL. There are many reports concerning ZnO toxicity against a variety of cell lines, including human erythrocytes, human keratinocytes, human lymphocytes, among other cell lines [90]. Literature reports on *in vitro* cytotoxicity evaluation of ZnO nanoparticles have a consensus for low toxicity on mammalian cells at a microscale for concentrations equal or less than 100 µg/mL.[90,91] Low surface area also seems to contribute to lower toxicity as is the case of BNC-ZnO hybrid film synthesized by Dincă *et al.* (2020). MTS assay with samples containing 1.68

μg ZnO NPs/mm^2 demonstrated high cell viability compared to bacterial cellulose alone and the control (human dermal fibroblast cells only).[68] A direct correlation between increase in antibacterial efficiency, size, as well as the concentration of ZnO NPs, has also been established in recent literature.[12,91]

In fact, recent cytotoxicity screening tests for engineered nanomaterials including ZnO nanoparticles described them as having cytotoxic effects with a half maximal inhibitory concentration no higher than 50 μg/mL on THP.1 cells with induced differentiation, *via* Alamar Blue assay.[92] From the study of Kocbek *et al.* (2010), a concentration as low as 15 μg/mL is enough to exert cytotoxic effects on human keratinocytes, for short-term exposure.[93] In contrast, other studies report with reported non-toxicity at concentrations up to 100 μg/mL of micro and nanoparticles of ZnO.[91]

From these reports it can be considered that the ZnO particles evaluated in this assay begin to have a cytotoxity effect at a concentration that is within the expected range of previously reported values (between 15 μg/mL and 100 μg/mL for micro and nanoparticles of this metal oxide).[91–93]

Considering possible factors that may explain the cytotoxicity of prepared hybrids, namely, **HS6** and **HS8**, and, observing that all prepared hybrids from hydrothermal and sol-gel synthesis had a pH of 9, approximately, a comparison between **HS8** with and without dialysis was made in this assay (Figure 25).

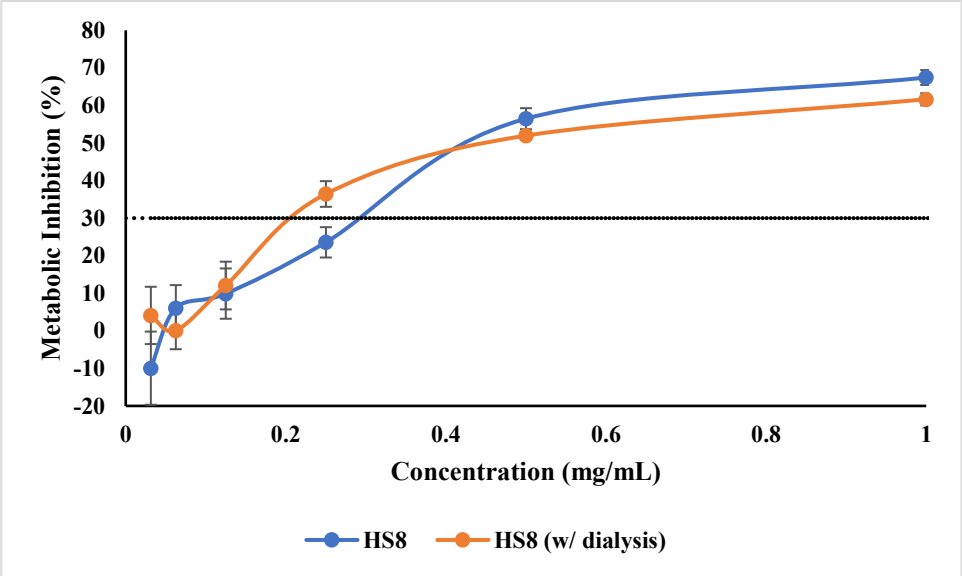

Figure 25. Graph of **HS8** with dialysis (pH=7.4) and **HS8** without dialysis (pH=9) concentrations plotted against respective metabolic inhibition effect on HaCaT cells. The dotted line represents the 30% cytotoxicity limit as defined by the ISO 10993-5:2.

HS8 with dialysis had a final pH of 7.4, similar to the physiological pH of the human body, which is in theory ideal for the maintenance of a prosperous environment for cell viability in most cell lines.[94,95]

In Figure 25, it is possible to see that HS8 material with or without dialysis didn't show a significant difference upon HaCaT cells metabolic activity, thus suggesting that the toxicity of the hybrids is not due to pH or to the presence of other compounds from the synthesis process.

Taking into consideration the results of CNC and ZnO alone, the observed cytotoxic response in studied HaCaT cells may be due to presence of the ZnO particles in the hybrids composition.

3.3.3. Wound healing assay

For the wound healing assay *via* scratch test, it was used a special plate with a gap between monolayer of cells, the ibidi® µ-Plate 24 Well Black ID 14 mm ibiTreat, mimicking a cell-free zone, similar to a wound area. The *in vitro* scratch assay allows the study of the samples' wound healing potential by observation of cell migration, compared against a basal control.[96,97]For proper migration detection the proliferation of HaCaT cells

has to be inhibited, which, in this case, was achieved by treatment with Mitomycin C, an antineoplastic drug with antiproliferative effects.[98,99]

The cytotoxicity evaluation carried out in this work was used to define the safe concentrations of materials for the assay. The following concentrations were prepared: 20 µg/mL of ZnO, 200 µg/mL of CNC (duplicates), 50 µg/mL of CNC, 200 µg/mL of **HS8** and **HS6** (duplicates) and 50 µg/mL of both **HS8** and **HS6**. These concentrations were chosen considering the values where the hybrid materials and construction units' samples didn't exert cytotoxic effects, according to the PrestoBlue assay. Figure 26 contains the main results of wound healing assay.

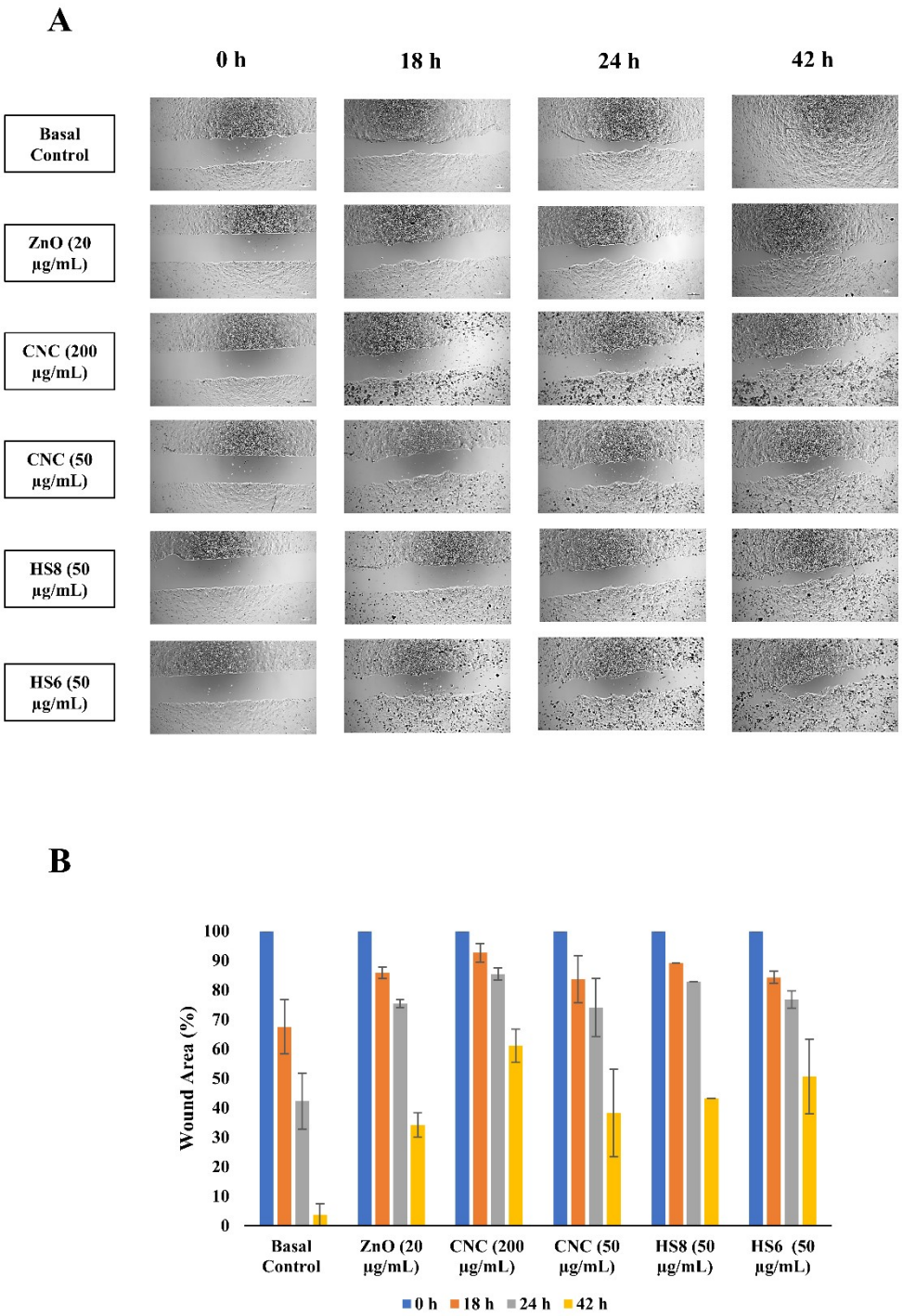

Figure 26. A) Photographs obtained for wound area contraction upon contact with ZnO (20 µg/mL), CNC (at 50 and 200 µg/mL), **HS8** and **HS6** (at 50 µg/mL) hybrid materials at 0, 18, 24 and 42 h by Zen software (Zeiss). **B**) Graph with average values and standard

deviation for wound area percentage for ZnO (20 µg/mL), CNC (at 50 and 200 µg/mL), and **HS8** and **HS6** (at 50 µg/mL) materials at 0, 18, 24 and 42 h .

Results from wound healing assay for materials **HS6** and **HS8** at 200 µg/mL showed some cell death (data not shown). As such, Figure 26 only contemplates the basal control, and all the material samples where wound area contraction was be observed.

The basal control suffered a significant wound area contraction, ca. 60% over 24 h and practically total contraction over 42 h. It was the fastest condition to close the wound.

ZnO sample at 20 µg/mL displayed significant cell migration rate with 34 % of wound area contraction over 42 h. Samples of CNC at 200 µg/mL and **HS6** at 50 µg/mL had a relatively similar wound contraction rate, with ca. 60 % and 50 % of wound area contracted over 42 h, respectively. On the other hand, CNC and **HS8** at 50 µg/mL displayed a lower cell migration rate, presenting a wound contraction rate of 38% and 43 % of wound area over 42 h, respectively.

Taking into consideration the rate of wound closure of the analyzed materials compared against the performance of the basal control, the developed materials exerted the wound contraction up to some extent, however they did show total wound contraction, so a inhibition in cell migration was caused, therefore they didn't present wound healing potential.

There are reports in literature on ZnO nanoparticles or ZnO-based hybrid materials with wound healing potential from both *in vivo* and *in vitro* experiments including investigation of biological activity in rats, quantification of the expression of growth factors and pro-inflammatory cytokines and other inflammatory mediators, wound healing rate and others. Even so, they differ from this work in the sense that promotion of wound healing wasn't attributed solely to cellular migration, being, instead, supported by the promotion of wound healing rate compared to reference controls, reduction of the expression of pro-inflammatory cytokines, observation of reduced hypoxia and oxidative stress, among other events related to wound healing.[71,100–102]

In the present work, the hybrid materials showed inhibition of cell migration, which promotes the process of wound healing. Interestingly, there is one report from Sonntag *et al.* (2022) pertaining to the use of ZnO tetrapods, a form of ZnO nanoparticles, as modulators for wound healing in an *in vitro* environment which also reported wound healing inhibition. The authors indicated possible application as an anti-inflammatory

agent due to observing inhibition of proteins that promote inflammation, namely cytokines, as an innovative approach for development of coating materials that modulate wound healing.[100] Molecular mechanisms that may be at play for inhibition of cell migration with the evaluated samples, still need to be further explored and characterized, for a better comprehension of the hybrid materials and construction units' effect on the studied cell line. With the work of Lee *et al.* (2018), it is proposed that certain signaling pathways that regulate reactive species of oxygen activity may inhibit cell migration.[101]

In line to the aforementioned observations, the results obtained through this study showed that zinc oxide particles did not directly take part in the migration process of the analyzed keratinocytes, an event that promotes wound healing as previously discussed in this work. As such, to further explore wound healing potential of the evaluated materials, other *in vitro* and *in vivo* experiments should be employed: study of antibacterial activity, which in theory promotes wound healing since bacterial infections delay the process; epithelization; angiogenesis; collagen deposition and other related events relevant to wound healing processes.[98,102]

4. Conclusion

In this work CNC/ZnO hybrids were prepared through *in-situ* approaches, where CNC exhibited a double function, acting as a reducting agent and as a support matrix, *via* hydrothermal and sol-gel methods. Those methods were chosen due to reported advantages such as high purity and crystallinity of synthesized products, repeatability and ease of execution as well as minimal reagents requirement and mild reactions making for a more environmentally-friendly process. The successful obtention of the hybrid materials was investigated by UV-Vis spectroscopy, and the structural features were studied by ATR-FT-IR; PXRD, and electronic microscopy. The CNC/ZnO hybrid that revealed to be stable and distinct structural properties were selected to be evaluated in wound healing.

In the preparation of the hybrid materials, using the *in-situ* hydrothermal process were obtained the materials **HS1**-**HS8**. While the process to attain the materials **HS1** and **HS2** revealed issues in the collection of the material after the reaction to further processing, the process to obtain the materials **HS3**-**HS8** revealed to be robust, without any complication regarding the obtention of the desired materials. In the *in-situ* hydrothermal process was investigated the following set of reaction conditions: utilization

of different zinc salts ($ZnCl_2$ and $Zn(CH_3COOH)_2.2H_2O$); different ratios of CNC/Zinc salt/NaOH, and different reaction temperature and time.

On the other hand, by the sol-gel methodology, were obtained the materials **SG1**-**SG3**, where different ratios of CNC/ $Zn(CH_3COOH)_2.2H_2O$ were studied.

The successful obtention of the hybrid materials **HS3**-**HS8** and **SG1**-**SG3** was confirmed by UV-Vis spectroscopy. The materials (**HS5**-**HS8** and **SG3**) showed a characteristic peak (360/370 nm), as expected from literature reports, confirming the obtention of the desired products. For the CNC/ZnO hybrid materials **HS3**-**HS4**, and **SG1**-**SG2** was observed a blue shift (change in absorbance that occurs at the wavelength of 300 nm), when compared with the previous data obtained, which may be associated with a decrease in the size of ZnO in the hybrid materials.

The structural features of the CNC/ZnO materials obtained by hydrothermal (**HS3**-**HS8**) and sol-gel (**SG1**-**SG3**) *in-situ* approaches were evaluated by ATR-FT-IR spectroscopy, PXRD analysis and electronic microscopy (SEM and TEM).

By ATR-FT-IR spectroscopy, it was possible to observe the characteristic vibrations of the CNC building unit. The PXRD analysis allowed to obtain the PXRD patterns for all mentioned hybrid materials (**HS3**-**HS8** and **SG1**-**SG3**), and the comparison with the PXRD patterns attained for the CNC building unit, and for a commercial sample of ZnO. In all CNC/ZnO materials, the characteristic reflections of CNC and ZnO were present, corroborating the successful obtention of the hybrid materials. This technique also allowed the study of crystallinity and to make assumptions regarding the crystal size.

The morphological study for the hybrid materials was performed by SEM (**HS3**-**HS8** and **SG1**-**SG3**) and by TEM (**HS6** and **HS8**) – in both cases the morphology of the obtained materials was compared with the morphology of the CNC building unit, and with the morphology of a commercial nanopowder of ZnO.

The variety of morphologies present in material **HS8** indicate that the sea urchin-like morphology of ZnO is a transitory state for the flower-like morphology that was observed from SEM and TEM microscopy images. In line to this assessment, material **HS6** presented with nanorod-like morphology on TEM microscopy analysis and the remaining hydrothermal materials (**HS3**-**HS5** and **HS7**) presented with irregular agglomerates of ZnO from SEM evaluation.

SEM images of sol-gel materials denote the formation of irregular agglomerates of ZnO and, according to SEM analysis, formation of bigger agglomerates occurred in

hybrids from sol-gel preparation (**SG1**-**SG3**) in comparison to the ones from hydrothermal synthesis (**HS3**-**HS8**), which may be due to the synthesis method employed.

Cytotoxicity evaluation revealed that CNC displayed non-toxicity which was according to previous reports on biocompatibility of other forms of nanocellulose. Developed hybrid compounds, namely materials **HS6** and **HS8**, did not exert toxicity for concentrations up to 0.0625 mg/mL and 0.25 mg/mL, respectively.

Finally, to conclude, the wound healing assay shows that there was no significant wound healing potential for evaluated hybrid materials since cell migration was inhibited compared to basal control.

In sum, considering the main findings from the hybrid materials preparation, structural characterization and biological evaluation, lower concentrations of the materials chosen for wound healing study shall be tested to further explore the effect of compounds' concentration on cell migration.

5. Future Work

In an effort to further characterize the prepared hybrids contemplated in this work, as well as to explore other possible potential applications according to the hybrid materials' properties, further characterization analyses will be employed:

-ZnO distribution on the different hybrids *via* elemental analysis and LIBS technology;

-zinc and sulfur distribution on the different materials through EDS (Energy-dispersive X-ray Spectroscopy) mapping;

-thermal (TGA, also known as thermogravimetric analysis) and structural materials' stability;

- The structure determination of the hybrid material with the highest biological potention will be determined by Single-crystal X-Ray Diffraction.

In line to this assessment, lower concentrations of the hybrids should be tested for evaluation of wound healing potential considering the results obtained herein.

References

1. Ananikov VP. Organic–Inorganic Hybrid Nanomaterials. Vol. 9, Nanomaterials. 2019.

2. Kuddushi M, Shah AA, Ayranci C, Zhang XH. Recent advances in novel materials and techniques for developing transparent wound dressings. J Mater Chem B. 2023;

3. Oun AA, Shankar S, Rhim JW. Multifunctional nanocellulose/metal and metal oxide nanoparticle hybrid nanomaterials. Crit Rev Food Sci Nutr [Internet]. 2020 Feb 4;60(3):435–60. Available from: https://doi.org/10.1080/10408398.2018.1536966

4. Predoi D, Iconaru SL, Buton N, Badea ML, Marutescu L. Antimicrobial Activity of New Materials Based on Lavender and Basil Essential Oils and Hydroxyapatite. Vol. 8, Nanomaterials. 2018.

5. Yoon GJ, Lee SY, Lee SB, Park GY, Choi JH. Synthesis of Iron Oxide/Gold Composite Nanoparticles Using Polyethyleneimine as a Polymeric Active Stabilizer for Development of a Dual Imaging Probe. Vol. 8, Nanomaterials. 2018.

6. Evdokimova OL, Svensson FG, Agafonov A V, Håkansson S, Seisenbaeva GA, Kessler VG. Hybrid Drug Delivery Patches Based on Spherical Cellulose Nanocrystals and Colloid Titania—Synthesis and Antibacterial Properties. Vol. 8, Nanomaterials. 2018.

7. Web of Science™ [Internet]. [cited 2023 Jul 4]. Available from: https://www.webofscience.com/wos/woscc/summary/9ddc1dba-fbf2-4a00-8852-90bce101d850-989e9c18/relevance/1

8. Abdul Khalil HPS, Tye YY, Leh CP, Saurabh CK, Ariffin F, Mohammad Fizree H, et al. Cellulose Reinforced Biodegradable Polymer Composite Film for Packaging Applications BT - Bionanocomposites for Packaging Applications. In: Jawaid M, Swain SK, editors. Cham: Springer International Publishing; 2018. p. 49–69. Available from: https://doi.org/10.1007/978-3-319-67319-6_3

9. Zhang H, Yu HY, Wang C, Yao J. Effect of silver contents in cellulose nanocrystal/silver nanohybrids on PHBV crystallization and property improvements. Carbohydr Polym [Internet]. 2017;173:7–16. Available from: https://www.sciencedirect.com/science/article/pii/S0144861717305817

10. Cheng D, Wen Y, An X, Zhu X, Ni Y. TEMPO-oxidized cellulose nanofibers (TOCNs) as a green reinforcement for waterborne polyurethane coating (WPU) on wood. Carbohydr Polym [Internet]. 2016;151:326–34. Available from: https://www.sciencedirect.com/science/article/pii/S0144861716306130

11. Yu H, Sun B, Zhang D, Chen G, Yang X, Yao J. Reinforcement of biodegradable poly(3-hydroxybutyrate-co-3-hydroxyvalerate) with cellulose nanocrystal/silver nanohybrids as bifunctional nanofillers. J Mater Chem B [Internet]. 2014;2(48):8479–89. Available from: http://dx.doi.org/10.1039/C4TB01372G

12. Oprea M, Panaitescu DM. Nanocellulose Hybrids with Metal Oxides Nanoparticles for Biomedical Applications. Vol. 25, Molecules. 2020.

13. An X, Long Y, Ni Y. Cellulose nanocrystal/hexadecyltrimethylammonium bromide/silver nanoparticle composite as a catalyst for reduction of 4-nitrophenol. Carbohydr Polym [Internet]. 2017;156:253–8. Available from: https://www.sciencedirect.com/science/article/pii/S0144861716310517

14. Xie YY, Hu XH, Zhang YW, Wahid F, Chu LQ, Jia SR, et al. Development and antibacterial activities of bacterial cellulose/graphene oxide-CuO nanocomposite films. Carbohydr Polym [Internet]. 2020;229:115456. Available from: https://www.sciencedirect.com/science/article/pii/S0144861719311245

15. Khan S, Ul-Islam M, Khattak WA, Ullah MW, Park JK. Bacterial cellulose-titanium dioxide nanocomposites: nanostructural characteristics, antibacterial mechanism, and biocompatibility. Cellulose [Internet]. 2015;22(1):565–79. Available from: https://doi.org/10.1007/s10570-014-0528-4

16. Sruthi S, Ashtami J, Mohanan P V. Biomedical application and hidden toxicity of Zinc oxide nanoparticles. Mater Today Chem [Internet]. 2018;10:175–86. Available from: https://www.sciencedirect.com/science/article/pii/S2468519418301976

17. Luo Z, Liu J, Lin H, Ren X, Tian H, Liang Y, et al. In situ Fabrication of Nano

ZnO/BCM Biocomposite Based on MA Modified Bacterial Cellulose Membrane for Antibacterial and Wound Healing. Int J Nanomedicine. 2020;15:1–15.

18. Singla R, Soni S, Kulurkar PM, Kumari A, S. M, Patial V, et al. In situ functionalized nanobiocomposites dressings of bamboo cellulose nanocrystals and silver nanoparticles for accelerated wound healing. Carbohydr Polym [Internet]. 2017;155:152–62. Available from: https://www.sciencedirect.com/science/article/pii/S0144861716310098

19. Noremylia MB, Hassan MZ, Ismail Z. Recent advancement in isolation, processing, characterization and applications of emerging nanocellulose: A review. Int J Biol Macromol [Internet]. 2022;206:954–76. Available from: https://www.sciencedirect.com/science/article/pii/S0141813022005347

20. Tahir D, Karim MR, Hu H, Naseem S, Rehan M, Ahmad M, et al. Sources, Chemical Functionalization, and Commercial Applications of Nanocellulose and Nanocellulose-Based Composites: A Review. Vol. 14, Polymers. 2022.

21. Barhoum A, Rastogi VK, Mahur BK, Rastogi A, Abdel-Haleem FM, Samyn P. Nanocelluloses as new generation materials: natural resources, structure-related properties, engineering nanostructures, and technical challenges. Mater Today Chem [Internet]. 2022;26:101247. Available from: https://www.sciencedirect.com/science/article/pii/S2468519422004761

22. Solhi L, Guccini V, Heise K, Solala I, Niinivaara E, Xu W, et al. Understanding Nanocellulose–Water Interactions: Turning a Detriment into an Asset. Chem Rev [Internet]. 2023 Mar 8;123(5):1925–2015. Available from: https://doi.org/10.1021/acs.chemrev.2c00611

23. Liu B, Cheng L, Yuan Y, Hu J, Zhou L, Zong L, et al. Liquid-crystalline assembly of spherical cellulose nanocrystals. Int J Biol Macromol [Internet]. 2023;242:124738. Available from: https://www.sciencedirect.com/science/article/pii/S014181302301632X

24. Omran AAB, Mohammed AABA, Sapuan SM, Ilyas RA, Asyraf MRM, Rahimian Koloor SS, et al. Micro- and Nanocellulose in Polymer Composite Materials: A Review. Vol. 13, Polymers. 2021.

25. Stepanova M, Korzhikova-Vlakh E. Modification of Cellulose Micro- and

Nanomaterials to Improve Properties of Aliphatic Polyesters/Cellulose Composites: A Review. Vol. 14, Polymers. 2022.

26. Foroughi F, Rezvani Ghomi E, Morshedi Dehaghi F, Borayek R, Ramakrishna S. A Review on the Life Cycle Assessment of Cellulose: From Properties to the Potential of Making It a Low Carbon Material. Vol. 14, Materials. 2021.

27. Trache D, Tarchoun AF, Derradji M, Hamidon TS, Masruchin N, Brosse N, et al. Nanocellulose: From Fundamentals to Advanced Applications. Front Chem [Internet]. 2020;8. Available from: https://www.frontiersin.org/articles/10.3389/fchem.2020.00392

28. TAPPI. Standard Terms and Their Definition for Cellulose Nanomaterial. ISO/TS 20477:2017. Geneva, Switzerland; 2017.

29. Gorbunova M, Grunin L, Morris RH, Imamutdinova A. Nanocellulose-Based Thermoplastic Polyurethane Biocomposites with Shape Memory Effect. Vol. 7, Journal of Composites Science. 2023.

30. Huo Y, Liu Y, Xia M, Du H, Lin Z, Li B, et al. Nanocellulose-Based Composite Materials Used in Drug Delivery Systems. Vol. 14, Polymers. 2022.

31. Shazali NA, Zaidi NE, Ariffin H, Abdullah LC, Ghaemi F, Abdullah JM, et al. Characterization and Cellular Internalization of Spherical Cellulose Nanocrystals (CNC) into Normal and Cancerous Fibroblasts. Vol. 12, Materials. 2019.

32. Casanova F, Pereira CF, Ribeiro AB, Freixo R, Costa E, E. Pintado M, et al. Novel Micro- and Nanocellulose-Based Delivery Systems for Liposoluble Compounds. Vol. 11, Nanomaterials. 2021.

33. Randhawa A, Dutta SD, Ganguly K, Patil T V, Patel DK, Lim KT. A Review of Properties of Nanocellulose, Its Synthesis, and Potential in Biomedical Applications. Vol. 12, Applied Sciences. 2022.

34. Kannan K, Radhika D, Sadasivuni KK, Reddy KR, Raghu A V. Nanostructured metal oxides and its hybrids for photocatalytic and biomedical applications. Adv Colloid Interface Sci [Internet]. 2020;281:102178. Available from: https://www.sciencedirect.com/science/article/pii/S0001868620302360

35. Farooq A, Patoary MK, Zhang ML, Mussana H, Li MM, Naeem MA, et al.

Cellulose from sources to nanocellulose and an overview of synthesis and properties of nanocellulose/zinc oxide nanocomposite materials. Int J Biol Macromol. 2020;154:1050–73.

36. Lizundia E, Goikuria U, Vilas JL, Cristofaro F, Bruni G, Fortunati E, et al. Metal Nanoparticles Embedded in Cellulose Nanocrystal Based Films: Material Properties and Post-use Analysis. Biomacromolecules [Internet]. 2018 Jul 9;19(7):2618–28. Available from: https://doi.org/10.1021/acs.biomac.8b00243

37. Mirtalebi SS, Almasi H, Alizadeh Khaledabad M. Physical, morphological, antimicrobial and release properties of novel MgO-bacterial cellulose nanohybrids prepared by in-situ and ex-situ methods. Int J Biol Macromol [Internet]. 2019;128:848–57. Available from: https://www.sciencedirect.com/science/article/pii/S0141813018362767

38. Galkina OL, Önneby K, Huang P, Ivanov VK, Agafonov A V, Seisenbaeva GA, et al. Antibacterial and photochemical properties of cellulose nanofiber–titania nanocomposites loaded with two different types of antibiotic medicines. J Mater Chem B [Internet]. 2015;3(35):7125–34. Available from: http://dx.doi.org/10.1039/C5TB01382H

39. Shankar S, Rhim JW. Amino acid mediated synthesis of silver nanoparticles and preparation of antimicrobial agar/silver nanoparticles composite films. Carbohydr Polym [Internet]. 2015;130:353–63. Available from: https://www.sciencedirect.com/science/article/pii/S0144861715004166

40. Maruthupandy M, Zuo Y, Chen JS, Song JM, Niu HL, Mao CJ, et al. Synthesis of metal oxide nanoparticles (CuO and ZnO NPs) via biological template and their optical sensor applications. Appl Surf Sci [Internet]. 2017;397:167–74. Available from: https://www.sciencedirect.com/science/article/pii/S0169433216324862

41. Wasim M, Shi F, Liu JX, Farooq A, Khan SU, Salam A, et al. An overview of Zn/ZnO modified cellulosic nanocomposites and their potential applications. J Polym Res. 2021;28(9).

42. Montazer M, Maali Amiri M. ZnO Nano Reactor on Textiles and Polymers: Ex Situ and In Situ Synthesis, Application, and Characterization. J Phys Chem B

[Internet]. 2014 Feb 13;118(6):1453–70. Available from: https://doi.org/10.1021/jp408532r

43. Guo Q, Ghadiri R, Weigel T, Aumann A, Gurevich EL, Esen C, et al. Comparison of in Situ and ex Situ Methods for Synthesis of Two-Photon Polymerization Polymer Nanocomposites. Vol. 6, Polymers. 2014. p. 2037–50.

44. Kołodziejczak-Radzimska A, Jesionowski T. Zinc Oxide—From Synthesis to Application: A Review. Vol. 7, Materials. 2014. p. 2833–81.

45. Zhou XQ, Hayat Z, Zhang DD, Li MY, Hu S, Wu Q, et al. Zinc Oxide Nanoparticles: Synthesis, Characterization, Modification, and Applications in Food and Agriculture. Vol. 11, Processes. 2023.

46. Carter CB, Norton MG, editors. Sols, Gels, and Organic Chemistry BT - Ceramic Materials: Science and Engineering. In New York, NY: Springer New York; 2007. p. 400–11. Available from: https://doi.org/10.1007/978-0-387-46271-4_22

47. Bokov D, Turki Jalil A, Chupradit S, Suksatan W, Javed Ansari M, Shewael IH, et al. Nanomaterial by Sol-Gel Method: Synthesis and Application. Wang Z, editor. Adv Mater Sci Eng [Internet]. 2021;2021:5102014. Available from: https://doi.org/10.1155/2021/5102014

48. Devasia R, Painuly A, Devapal D, Sreejith KJ. 22 - Continuous fiber reinforced ceramic matrix composites. In: Joseph K, Oksman K, George G, Wilson R, Appukuttan SBTFRC, editors. Woodhead Publishing Series in Composites Science and Engineering [Internet]. Woodhead Publishing; 2021. p. 669–751. Available from: https://www.sciencedirect.com/science/article/pii/B9780128210901000223

49. Jimenez-Cadena G, Comini E, Ferroni M, Vomiero A, Sberveglieri G. Synthesis of different ZnO nanostructures by modified PVD process and potential use for dye-sensitized solar cells. Mater Chem Phys [Internet]. 2010;124(1):694–8. Available from: https://www.sciencedirect.com/science/article/pii/S0254058410005821

50. Müller R, Huber F, Gelme O, Madel M, Scholz JP, Minkow A, et al. Chemical Vapor Deposition Growth of Zinc Oxide on Sapphire with Methane: Initial

Crystal Formation Process. Cryst Growth Des [Internet]. 2019 Sep 4;19(9):4964–9. Available from: https://doi.org/10.1021/acs.cgd.9b00181

51. Lv H, Sang DD, Li HD, Du XB, Li DM, Zou GT. Thermal Evaporation Synthesis and Properties of ZnO Nano/Microstructures Using Carbon Group Elements as the Reducing Agents. Nanoscale Res Lett [Internet]. 2010;5(3):620. Available from: https://doi.org/10.1007/s11671-010-9524-2

52. Stanković A, Veselinović L, Škapin SD, Marković S, Uskoković D. Controlled mechanochemically assisted synthesis of ZnO nanopowders in the presence of oxalic acid. J Mater Sci [Internet]. 2011;46(11):3716–24. Available from: https://doi.org/10.1007/s10853-011-5273-6

53. Muhammad W, Ullah N, Haroon M, Abbasi BH. Optical, morphological and biological analysis of zinc oxide nanoparticles (ZnO NPs) using Papaver somniferum L. RSC Adv [Internet]. 2019;9(51):29541–8. Available from: http://dx.doi.org/10.1039/C9RA04424H

54. Ogunyemi SO, Abdallah Y, Zhang M, Fouad H, Hong X, Ibrahim E, et al. Green synthesis of zinc oxide nanoparticles using different plant extracts and their antibacterial activity against Xanthomonas oryzae pv. oryzae. Artif Cells, Nanomedicine, Biotechnol [Internet]. 2019 Dec 4;47(1):341–52. Available from: https://doi.org/10.1080/21691401.2018.1557671

55. Divya B, Karthikeyan C, Rajasimman M. Chemical Synthesis of Zinc Oxide Nanoparticles and Its Application of Dye Decolourization. Int J Nanosci Nanotechnol [Internet]. 2018;14(4):267–75. Available from: https://www.ijnnonline.net/article_33274.html

56. Brandes R, de Souza L, Vargas V, Oliveira E, Mikowski A, Carminatti C, et al. Preparation and Characterization of Bacterial Cellulose/TiO2 Hydrogel Nanocomposite. J Nano Res [Internet]. 2016;43:73–80. Available from: https://www.scientific.net/JNanoR.43.73

57. Boboc M, Curti F, Fleacă AM, Jianu ML, Roşu AM, Curutiu C, et al. Chapter 14 - Preparation and Antimicrobial Activity of Inorganic Nanoparticles: Promising Solutions to Fight Antibiotic Resistance. In: Ficai A, Grumezescu AMBTN for AT, editors. Micro and Nano Technologies [Internet]. Elsevier; 2017. p. 325–40.

Available from:
https://www.sciencedirect.com/science/article/pii/B9780323461528000147

58. Abdalkarim SYH, Yu HY, Wang C, Yang L, Guan Y, Huang L, et al. Sheet-like Cellulose Nanocrystal-ZnO Nanohybrids as Multifunctional Reinforcing Agents in Biopolyester Composite Nanofibers with Ultrahigh UV-Shielding and Antibacterial Performances. ACS Appl Bio Mater [Internet]. 2018 Sep 17;1(3):714–27. Available from: https://doi.org/10.1021/acsabm.8b00188

59. Xiong R, Wang Y, Zhang X, Lu C. Facile synthesis of magnetic nanocomposites of cellulose@ultrasmall iron oxide nanoparticles for water treatment. RSC Adv [Internet]. 2014;4(43):22632–41. Available from: http://dx.doi.org/10.1039/C4RA01397B

60. Pavón JJ, Allain JP, Verma D, Echeverry-Rendón M, Cooper CL, Reece LM, et al. In situ Study Unravels Bio-Nanomechanical Behavior in a Magnetic Bacterial Nano-cellulose (MBNC) Hydrogel for Neuro-Endovascular Reconstruction. Macromol Biosci [Internet]. 2019 Feb 1;19(2):1800225. Available from: https://doi.org/10.1002/mabi.201800225

61. Guan Y, Yu HY, Abdalkarim SYH, Wang C, Tang F, Marek J, et al. Green one-step synthesis of ZnO/cellulose nanocrystal hybrids with modulated morphologies and superfast absorption of cationic dyes. Int J Biol Macromol [Internet]. 2019;132:51–62. Available from: https://www.sciencedirect.com/science/article/pii/S0141813018372878

62. Kumar A, Gullapalli H, Balakrishnan K, Botello-Mendez A, Vajtai R, Terrones M, et al. Flexible ZnO–Cellulose Nanocomposite for Multisource Energy Conversion. Small [Internet]. 2011 Aug 8;7(15):2173–8. Available from: https://doi.org/10.1002/smll.201100458

63. Abdalkarim SYH, Yu H, Wang C, Chen Y, Zou Z, Han L, et al. Thermo and light-responsive phase change nanofibers with high energy storage efficiency for energy storage and thermally regulated on–off drug release devices. Chem Eng J [Internet]. 2019;375:121979. Available from: https://www.sciencedirect.com/science/article/pii/S1385894719313737

64. Jia M, Zhang X, Weng J, Zhang J, Zhang M. Protective coating of paper works:

ZnO/cellulose nanocrystal composites and analytical characterization. J Cult Herit [Internet]. 2019;38:64–74. Available from: https://www.sciencedirect.com/science/article/pii/S1296207418302255

65. Lefatshe K, Muiva CM, Kebaabetswe LP. Extraction of nanocellulose and in-situ casting of ZnO/cellulose nanocomposite with enhanced photocatalytic and antibacterial activity. Carbohydr Polym [Internet]. 2017;164:301–8. Available from: https://www.sciencedirect.com/science/article/pii/S0144861717301406

66. Katepetch C, Rujiravanit R, Tamura H. Formation of nanocrystalline ZnO particles into bacterial cellulose pellicle by ultrasonic-assisted in situ synthesis. Cellulose [Internet]. 2013;20(3):1275–92. Available from: https://doi.org/10.1007/s10570-013-9892-8

67. Khalid A, Khan R, Ul-Islam M, Khan T, Wahid F. Bacterial cellulose-zinc oxide nanocomposites as a novel dressing system for burn wounds. Carbohydr Polym [Internet]. 2017;164:214–21. Available from: https://www.sciencedirect.com/science/article/pii/S0144861717300723

68. Dincă V, Mocanu A, Isopencu G, Busuioc C, Brajnicov S, Vlad A, et al. Biocompatible pure ZnO nanoparticles-3D bacterial cellulose biointerfaces with antibacterial properties. Arab J Chem [Internet]. 2020;13(1):3521–33. Available from: https://www.sciencedirect.com/science/article/pii/S1878535218302533

69. Janpetch N, Saito N, Rujiravanit R. Fabrication of bacterial cellulose-ZnO composite via solution plasma process for antibacterial applications. Carbohydr Polym [Internet]. 2016;148:335–44. Available from: https://www.sciencedirect.com/science/article/pii/S0144861716304349

70. Wahid F, Duan YX, Hu XH, Chu LQ, Jia SR, Cui JD, et al. A facile construction of bacterial cellulose/ZnO nanocomposite films and their photocatalytic and antibacterial properties. Int J Biol Macromol [Internet]. 2019;132:692–700. Available from: https://www.sciencedirect.com/science/article/pii/S0141813019304003

71. Melnikova N, Knyazev A, Nikolskiy V, Peretyagin P, Belyaeva K, Nazarova N, et al. Wound Healing Composite Materials of Bacterial Cellulose and Zinc Oxide Nanoparticles with Immobilized Betulin Diphosphate. Vol. 11, Nanomaterials.

2021.

72. Ul-Islam M, Khattak WA, Ullah MW, Khan S, Park JK. Synthesis of regenerated bacterial cellulose-zinc oxide nanocomposite films for biomedical applications. Cellulose [Internet]. 2014;21(1):433–47. Available from: https://doi.org/10.1007/s10570-013-0109-y

73. Trindade NCTMANCTMACSRFACPNAAJDSAJCAGBAPSAT. Antibacterial paper based on composite coatings of nanofibrillated cellulose and ZnO. Colloids Surfaces A Physicochem Eng Asp [Internet]. 2013;v. 417:111-119–2013 v.417. Available from: http://dx.doi.org/10.1016/j.colsurfa.2012.10.042

74. Azizi S, Ahmad M, Mahdavi Shahri M, Abdolmohammadi S. Preparation, Characterization, and Antimicrobial Activities of ZnO Nanoparticles/Cellulose Nanocrystal Nanocomposites. BioResources. 2013 Jan 31;8.

75. Sahoo K, Mohanty B, Biswas A, Nayak J. Role of hexamethylenetetramine in ZnO-cellulose nanocomposite enabled UV and humidity sensor. Mater Sci Semicond Process [Internet]. 2020;105:104699. Available from: https://www.sciencedirect.com/science/article/pii/S1369800119311989

76. Shefa AA, Taz M, Hossain M, Kim YS, Lee SY, Lee BT. Investigation of efficiency of a novel, zinc oxide loaded TEMPO-oxidized cellulose nanofiber based hemostat for topical bleeding. Int J Biol Macromol [Internet]. 2019 Apr;126:786–95. Available from: https://www.sciencedirect.com/science/article/pii/S0141813018351328

77. Wahyuono RA, Schmidt C, Dellith A, Dellith J, Schulz M, Seyring M, et al. ZnO nanoflowers-based photoanodes: aqueous chemical synthesis, microstructure and optical properties. 2016;14(1):158–69. Available from: https://doi.org/10.1515/chem-2016-0016

78. Barua S, Das G, Aidew L, Buragohain AK, Karak N. Copper–copper oxide coated nanofibrillar cellulose: a promising biomaterial. RSC Adv [Internet]. 2013;3(35):14997–5004. Available from: http://dx.doi.org/10.1039/C3RA42209G

79. Torkashvand N, Sarlak N. Fabrication of a dual T1 and T2 contrast agent for magnetic resonance imaging using cellulose nanocrystals/Fe3O4 nanocomposite.

Eur Polym J [Internet]. 2019;118:128–36. Available from: https://www.sciencedirect.com/science/article/pii/S0014305719301569

80. Nypelö T, Rodriguez-Abreu C, Rivas J, Dickey MD, Rojas OJ. Magneto-responsive hybrid materials based on cellulose nanocrystals. Cellulose [Internet]. 2014;21(4):2557–66. Available from: https://doi.org/10.1007/s10570-014-0307-2

81. A.G. Soares Silva F, Carvalho M, Bento de Carvalho T, Gama M, Poças F, Teixeira P. Antimicrobial activity of in-situ bacterial nanocellulose-zinc oxide composites for food packaging. Food Packag Shelf Life [Internet]. 2023;40:101201. Available from: https://www.sciencedirect.com/science/article/pii/S2214289423001783

82. Echeverry-Rendon M, Reece LM, Pastrana F, Arias SL, Shetty AR, Pavón JJ, et al. Bacterial Nanocellulose Magnetically Functionalized for Neuro-Endovascular Treatment. Macromol Biosci [Internet]. 2017 Jun 1;17(6):1600382. Available from: https://doi.org/10.1002/mabi.201600382

83. Hafez E, Hassan H, Elkady M, Salama E. Assessment Of Antibacterial Activity For Synthesized Zinc Oxide Nanorods Against Plant Pathogenic Strains. Int J Sci Technol Res. 2014 Sep 1;3:318–24.

84. Stanković A, Dimitrijević S, Uskoković D. Influence of size scale and morphology on antibacterial properties of ZnO powders hydrothemally synthesized using different surface stabilizing agents. Colloids Surfaces B Biointerfaces [Internet]. 2013;102:21–8. Available from: https://www.sciencedirect.com/science/article/pii/S0927776512004286

85. Yu HY, Chen GY, Wang YB, Yao JM. A facile one-pot route for preparing cellulose nanocrystal/zinc oxide nanohybrids with high antibacterial and photocatalytic activity. Cellulose [Internet]. 2015;22(1):261–73. Available from: https://doi.org/10.1007/s10570-014-0491-0

86. Casanova F, Pereira CF, Ribeiro AB, Costa EM, Freixo R, Castro PM, et al. Design of Innovative Biocompatible Cellulose Nanostructures for the Delivery and Sustained Release of Curcumin. Vol. 15, Pharmaceutics. 2023.

87. Aguayo MG, Fernández Pérez A, Reyes G, Oviedo C, Gacitúa W, Gonzalez R, et al. Isolation and Characterization of Cellulose Nanocrystals from Rejected Fibers

Originated in the Kraft Pulping Process. Vol. 10, Polymers. 2018.

88. Atkins P, Shriver DF, Overton TL. Shriver & Atkins- Inorganic Chemistry. 4th ed. Italy: W.H.Freeman and Company (New York); 2006.

89. Abdallah W, Kamal MR. Influence of process variables on physical characteristics of spray freeze dried cellulose nanocrystals. Cellulose [Internet]. 2018;25(10):5711–30. Available from: https://doi.org/10.1007/s10570-018-1975-0

90. Liao C, Jin Y, Li Y, Tjong SC. Interactions of Zinc Oxide Nanostructures with Mammalian Cells: Cytotoxicity and Photocatalytic Toxicity. Int J Mol Sci [Internet]. 2020;21(17). Available from: https://www.mdpi.com/1422-0067/21/17/6305

91. Babayevska N, Przysiecka Ł, Iatsunskyi I, Nowaczyk G, Jarek M, Janiszewska E, et al. ZnO size and shape effect on antibacterial activity and cytotoxicity profile. Sci Rep [Internet]. 2022;12(1):8148. Available from: https://doi.org/10.1038/s41598-022-12134-3

92. Bhattacharya K, Kilic G, Costa PM, Fadeel B. Cytotoxicity screening and cytokine profiling of nineteen nanomaterials enables hazard ranking and grouping based on inflammogenic potential. Nanotoxicology. 2017;11(6):809–26.

93. Kocbek P, Teskač K, Kreft ME, Kristl J. Toxicological Aspects of Long-Term Treatment of Keratinocytes with ZnO and TiO2 Nanoparticles. Small [Internet]. 2010;6(17):1908–17. Available from: https://onlinelibrary.wiley.com/doi/abs/10.1002/smll.201000032

94. Proksch E. pH in nature, humans and skin. J Dermatol [Internet]. 2018 Sep 1;45(9):1044–52. Available from: https://doi.org/10.1111/1346-8138.14489

95. Tucker AM, Johnson TN. Acid-base disorders: A primer for clinicians. Nutr Clin Pract [Internet]. 2022 Oct 1;37(5):980–9. Available from: https://doi.org/10.1002/ncp.10881

96. Kauanova S, Urazbayev A, Vorobjev I. The Frequent Sampling of Wound Scratch Assay Reveals the “Opportunity” Window for Quantitative Evaluation of

Cell Motility-Impeding Drugs. Front Cell Dev Biol [Internet]. 2021;9. Available from: https://www.frontiersin.org/articles/10.3389/fcell.2021.640972

97. Stamm A, Reimers K, Strauß S, Vogt P, Scheper T, Pepelanova I. In vitro wound healing assays – state of the art. 2016;17(1–2):79–87. Available from: https://doi.org/10.1515/bnm-2016-0002

98. Labbé A, Baudouin C. 91 - Modulation of Wound Healing: Choice of Antifibrosis Therapies. In: Shaarawy TM, Sherwood MB, Hitchings RA, Crowston JGBTG (Second E, editors. W.B. Saunders; 2015. p. 894–905. Available from: https://www.sciencedirect.com/science/article/pii/B9780702051937000911

99. AU - Vang Mouritzen M, AU - Jenssen H. Optimized Scratch Assay for In Vitro Testing of Cell Migration with an Automated Optical Camera. JoVE [Internet]. 2018;(138):e57691. Available from: https://www.jove.com/t/57691

100. Le VA, Trinh TX, Chien PN, Giang NN, Zhang XR, Nam SY, et al. Evaluation of the Performance of a ZnO-Nanoparticle-Coated Hydrocolloid Patch in Wound Healing. Vol. 14, Polymers. 2022.

101. Li P, Ruan L, Wang R, Liu T, Song G, Gao X, et al. Electrospun Scaffold of Collagen and Polycaprolactone Containing ZnO Quantum Dots for Skin Wound Regeneration. J Bionic Eng [Internet]. 2021;18(6):1378–90. Available from: https://doi.org/10.1007/s42235-021-00115-7

102. Blinov A V, Kachanov MD, Gvozdenko AA, Nagdalian AA, Blinova AA, Rekhman ZA, et al. Synthesis and Characterization of Zinc Oxide Nanoparticles Stabilized with Biopolymers for Application in Wound-Healing Mixed Gels. Vol. 9, Gels. 2023.

103. Sonntag SR, Gniesmer S, Gapeeva A, Adelung R, Cojocaru A, Mishra YK, et al. Zinc Oxide Tetrapods Modulate Wound Healing and Cytokine Release In Vitro—A New Antiproliferative Substance in Glaucoma Filtering Surgery. Vol. 12, Life. 2022.

104. Lee JJ, van de Ven RAH, Zaganjor E, Ng MR, Barakat A, Demmers JJPG, et al. Inhibition of epithelial cell migration and Src/FAK signaling by SIRT3. Proc Natl Acad Sci [Internet]. 2018 Jul 3;115(27):7057–62. Available from:

https://doi.org/10.1073/pnas.1800440115

105. Khan A ur R, Huang K, Jinzhong Z, Zhu T, Morsi Y, Aldalbahi A, et al. Exploration of the antibacterial and wound healing potential of a PLGA/silk fibroin based electrospun membrane loaded with zinc oxide nanoparticles. J Mater Chem B [Internet]. 2021;9(5):1452–65. Available from: http://dx.doi.org/10.1039/D0TB02822C

106. Kotian SR, Bhat KMR, Padma D, Pai KSR. Influence of traditional medicines on the activity of keratinocytes in wound healing: an in-vitro study. ACB [Internet]. 2019 Aug 26;52(3):324–32. Available from: http://dx.doi.org/10.5115/acb.19.009